INFLUENCE OF CURING CONDITIONS AND WIDTH

ON THE FRACTURE OF CONCRETE BEAMS

by

Yu-Cheng Kan

B.S., Chung-Hsing University, Taiwan, 1985

A MASTER'S THESIS

submitted in partial fulfillment of the

requirements for the degree of

MASTER OF SCIENCE
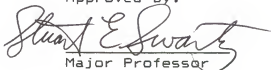
Department of Civil Engineering

KANSAS STATE UNIVERSITY

Manhattan, Kansas

1989

Approved by:

Major Professor

TABLE OF CONTENTS   A11208 315387

i

ACKNOWLEDGEMENTS

The author would like to express his appreciation to Dr. Stuart E. Swartz for his enlightenment and assistance during the period of research and preparation of this thesis.

Thanks are extended to Dr. Robert Snell, head of the Department of Civil Engineering, for his continual support during this research.

Also, the author is sincerely grateful to Mr. Liu and Mr. Luo, who volunteered to spend almost a summer period aiding the author's experimental work. In addition, thanks go to Mr. Ali Nikeen, Mr. Russell Gillespi, Miss Sze Ting Yap and Mr. Hoi Choong Siew for their expert suggestions that helped the author overcome numerous difficulties in the experiment.

Further and special gratitude is given to the author's families for their encouragement during the course of graduate study, especially the author's wife who provided a comfortable and supportive situation to finish this thesis.

LIST OF TABLES

LIST OF FIGURES

NOTATION

a, a_i, a_e	Crack Length, Initial Crack Length, Extended Crack Length
a_{oi}	Distance from The Crack "Mouth" to The Root of The "V-Shape" revealed by The Dye Penetrant
B	Beam Width
CMOD	Crack-Mouth-Opening Displacement
$CTOD_c$	Critical-Crack-Tip-Opening Displacement
E_c, E_t	Young's Modulus of Concrete in Compression and Tension
$f_c{}'$	Uniaxial Compressive Strength of Concrete
$f_{tw}{}'$, $f_{tn}{}'$	Splitting Tensile Strength of Concrete, Using Wide Strip, Narrow Strip Between Cylinder and Testing Surfaces
$f_r{}'$	Modulus of Rupture
g	Maximum Aggregate Size
G_{IC}	Energy Release Rate
J	J-Integral Value for Mode I Fracture
J_{IC}	Energy Release Rate by J-Integral Method
K_{IC}	Opening Mode Fracture Toughness or Critical Stress Intensity Factor
LPD	Load-Point Displacement
M	Moment Due to Three-Point Bending
N	Number of Segments by The Energy Release Method
P, P_m	Applied Load, Maximum Load or Load Capacity
S	Beam Span
r, θ	Polar Coordinates
U, U_t	Total Elastic Energy
V	Potential Energy

CHAPTER 1

Introduction

In the literature, to date, much research has been reported dealing with curing conditions on the subsequent strength of concrete; however, few reports mention this effect on the fracture properties of concrete. Until now, most of the fracture mechanics tests have dealt only with either air-dried specimens or saturated specimens. However, since several standard test methods have been proposed, the investigation of the influence of curing conditions on cracking and fracture of concrete can be conducted.

The research presented here evaluates the influences of size and curing conditions on the fracture of plain concrete using the methods of fracture mechanics. The analysis utilized herein is based on several proposed methods for the determination of fracture toughness and energy release rate.

The method developed by Go, Refai and Swartz (1, 2, 3) to determine the opening-mode fracture toughness K_{IC} was utilized; in addition, the energy release rate G_{IC} based on linear elastic fracture mechanics (LEFM) and using the calculated K_{IC} was carried out. Two other energy release rates based on the J-Integral method (2,4) and the method proposed by Refai (2, 5) were obtained to compare with the G_{IC}. Additionally, some specific beams with crack depth/beam depth ratio a_i/W of about 0.4 or 0.5 were used to

1

determine K_{IC} methods proposed by Jenq/Shah (6) and Nallathambi/Karihaloo (7). A detailed description of these methods is found in Chapter 4.

Two series of 36 beams each were made. Each beam series was classified into three groups for three specific curing conditions (i.e., oven-dried, air-dried and saturated). The three-point bending test was used throughout the experiment. The test specimens and test setups as well as the curing conditions are mentioned in Chapter 3.

Each beam was precracked and a dye technique was used (1, 2, 3) to reveal the crack shape of each precracked beam such that the crack growth could be predicted. As a result, the maximum load calibration method and the modified compliance calibration method (2, 3) could be applied to estimate any extended or effective crack length a_e from which the fracture toughness could be found through the three proposed formulas. In general, the results obtained from the three proposed methods are in agreement. The experimental and analytical results are shown in Chapter 4 and the conclusions and summaries are presented in Chapter 5.

CHAPTER 2

Literature Review

2.1 Proposed Methods for Fracture Toughness and Energy Release Rate

Since 1961, when Kaplan (8) first applied the concept of fracture mechanics to concrete, a great deal of research has been conducted to evaluate the fracture parameters for this material. It is believed that the stress intensity factor K should be a material property based on linear elastic fracture mechanics (LEFM). In opening mode (Mode I) fracture, a stress intensity factor K_I can be found which is related to the stress state at the crack tip. The critical vaule of this is associated with unstable crack growth and is referred to as the fracture toughness K_{IC}. This has been proposed as a fracture criterion of the material (1, 2, 3, 6, 7).

In the past years, several test methods using a three-point bending setup to evaluate the fracture toughness in the opening mode were developed and suggested to be standard methods. Jenq and Shah (6) used a direct method to calculate two size independent fracture parameters, i.e., critical stress intensity factor K_{IC} and critical crack tip opening displacement CTODc. This was done from the experimental results using single-edge-notched beams. One advantage of this method is that the post-peak (strain softening) constitutive law is not needed.

Nallathambi and Karihaloo (7) used an effective crack model to propose another direct method which is similar to the Jenq/Shah method. The fracture toughness K_{IC} and energy release rate G_{IC} were shown to be two parameters independent of the specimen dimensions. A regression formula based on a series of tests was developed to determine the extended crack length directly, so that no feedback control is required.

Go and Swartz (1) presented a modified compliance calibration method using a dye technique to reveal the crack surface of a precracked beam so as to obtain a nominal crack length, created by dividing the dyed area by the width of the beam. An effective crack length a_e, corresponding to the instability point, could be found using a compliance calculation technique. The mode I fracture toughness K_{IC} was estimated from a formula, derived from using the least squares method and based on the bending analogy analysis (9). The energy release rate G_{IC} was determined using the LEFM relation without considering Poisson's ratio. On the basis of this work, Refai (2, 3) refined the method by using a maximum load calibration technique to estimate the extended crack length in a consistent way. In addition, the results agreed with other proposed methods (6, 7).

Some other research based on the energy principle was developed to determine the energy release rate for concrete. Rice (10) developed the J-integral method which is applicable for either a linearly elastic or nonlinear

material. A parameter J_{IC} is considered to be the energy release rate with exactly the same meaning and value as G_{IC} if linear elastic fracture mechanics is valid. The only restriction when using this method is that unloading is not permitted. Based on this concept, Go presented a formula (2, 4) considering the roughness of the crack surface and determining the energy release rate directly by change in energy versus change in crack extension. The slope of the best line that fits the data gives the energy release rate, J_{IC}.

Refai also derived an energy release method (2, 5), using only the fundamental definition of energy release rate, G_{IC}. A practical formula was recommended for the calculation of the energy release rate G_{IC} from the load versus load-point-displacement (P-LPD) diagram. This is not necessarily an LEFM parameter. The maximum load versus compliance curve as well as the regression equation of maximum load versus crack length are required in this method.

2.2 Effects of Curing Conditions on The Fracture of Concrete

Up to now, rarely has research been presented relating to the investigation of the influence of curing conditions on the fracture properties of concrete, even though a great deal of similar work on the strength of concrete was reported in the literature.

5

Recently, Hordijk and Reinhart (11) presented results on tensile response and strength as influenced by curing conditions. Bazant and Prat (12) also have reported test results, using three-point bend and eccentric compression specimens, and evaluting the effects of temperature and humidity or water content on the Mode I fracture energy of concrete. The temperature effect was determined both for concrete predried in an oven and for saturated concrete. By interpolation, an approximate formula for the effect of moisture content on fracture energy was also obtained. It was found that the fracture energy of concrete significantly depends on temperature and that the effect of moisture content is small at room temperature but large at temperature close to 100°C (212°F). In addition, the size effect law (13) was verified to be applicable based on various specimens with similar geometry.

CHAPTER 3

Experimental Program

3.1 Test specimens

Two series of plain concrete beams were made in this experiment with the dimensions shown as follows:

    Series D: width, B = 3 in. (76 mm)
               depth, W = 8 in. (203 mm)
               span, S = 32 in. (813 mm)
               length, L = 34 in. (864 mm)

    Series E: width, B = 6 in. (152 mm)
               depth, W = 8 in. (203 mm)
               span, S = 32 in. (813 mm)
               length, L = 34 in. (864 mm)

Each series included 36 beams which were constructed using the mix design given in Table 3.1. In each series, the beam specimens were divided into three groups of 12, and each group was exposed to three specific curing conditions. The curing conditions were: one day in the plywood casting mold with a plastic sheet over the exposed surface and 30 days in a 100% humidity curing room, then

    a. Oven-dried: 60 days in an oven at 77°C (171°F),

    b. air-dried: 60 days in the laboratory environment,

    c. saturated: 60 additional days in the curing room.

Consequently, a total of six different groups were arranged, based on size (width) and curing condition. For convenience, the capital letters D and E are used to represent the narrow

7

beams of 3 in. width and the wide beams of 6 in. width,
respectively; hence, the beam number as well as each
pertaining group could be set up according to the following:

	Oven-dried	Air-dried	Saturated
Narrow	D1-D12	D13-D24	D25-D36
Wide	E1-E12	E13-E24	E25-E36

In addition, at least four cylinders of 3"x 6" (76 mm x
152 mm) were made in each batch to obtain the appropriate
properties of concrete. Two of the cylinders were taken for
compressive strength tests; one was for the measurement of
the moisture content of concrete and the rest were used for
the splitting test to obtain approximate tensile strength.

3.2 Testing Machine And Setups

An electro-hydraulic, closed-loop, materials testing
system (MTS) machine was used for all of the beam tests.
For some practical reason, the configuration utilized in
this research was designed as an upside-down, three-point
bend setup as shown schematically in Figure 3.1. At the
terminals (plotters) of the machine, the crack-mouth-opening
displacement (CMOD) and the load-point displacement (LPD)
were simultaneously monitored through two transducers with a
maximum sensitivity of ±0.002 in (0.0508 mm) per 10 volt full
scale output. A set of knife edges as shown in Fig. 3.2 was
bonded to the beam and used to contact with the CMOD
transducer at the notch. Also, the relative LPD was
measured by attaching the gage to the knife-edge-spring

setup which was attached on the side of the square steel
plate that fitted firmly around the moving piston. This is
shown in Fig. 3.3.

In MTS, there are three available control modes, i.e.,
load control, strain control and stroke control. Under load
control, the span (amplitude) responds to the amount of
load as the primary feedback with a constant load rate using
the ramp function. This control was used when loading the
specimens to failure. When using strain control, the span
responds to the displacement of the CMOD transducer as the
primary feedback, which makes it possible to crack the beam
to a desired depth with less danger of premature failure
since the rate of CMOD is more controllable than the load
rate. The stroke control, using the displacement of the
loading head as its primary feedback, was applied only for
the work of warm-up before testing.

To get the traces of the load versus CMOD as well as
LPD, appropriate scale settings on the plotters should be
selected. The plotters used were each MTS 431.13A-02 (Type
200 Control Module). A summary of X (load) and Y
(displacement) axis scale setting follows (cm refers to
plotted length):

X-axis Metric Setting

Ranges using calib. setting:

```
 0.5% per cm = 0.05 v/cm
 1.0% per cm = 0.10 v/cm
 2.5% per cm = 0.25 v/cm
 5.0% per cm = 0.50 v/cm
10.0% per cm = 1.00 v/cm
```

CMOD – Range 2, $\pm 1 \times 10^{-2}$ in./10 v = $\pm 1 \times 10^{-3}$ in./v

    0.5%: 1 cm = 5.0×10^{-5} in.
    1.0%: 1 cm = 1.0×10^{-4} in.
    2.5%: 1 cm = 2.5×10^{-4} in.
    5.0%: 1 cm = 5.0×10^{-4} in.

CMOD – Range 1, $\pm 2 \times 10^{-2}$ in./10 v = $\pm 2 \times 10^{-3}$ in./v

    0.5%: 1 cm = 1×10^{-4} in.
    1.0%: 1 cm = 2×10^{-4} in.
    2.5%: 1 cm = 5×10^{-4} in.
    5.0%: 1 cm = 1×10^{-3} in.

LPD – Range 2, $\pm 9.72 \times 10^{-4}$ in./v

    0.5%: 1 cm = 4.86×10^{-5} in.
    1.0%: 1 cm = 9.72×10^{-5} in.
    2.5%: 1 cm = 2.43×10^{-4} in.
    5.0%: 1 cm = 4.86×10^{-4} in.

LPD – Range 1, $\pm 19.08 \times 10^{-4}$ in./v

    0.5%: 1 cm = 9.54×10^{-5} in.
    1.0%: 1 cm = 19.08×10^{-5} in.
    2.5%: 1 cm = 4.77×10^{-4} in.
    5.0%: 1 cm = 9.54×10^{-4} in.

<u>Y-axis</u> Metric Setting:

Ranges using calib. setting:

    0.5% per cm = 0.05 v/cm
    1.0% per cm = 0.10 v/cm
    2.5% per cm = 0.25 v/cm
    5.0% per cm = 0.50 v/cm
   10.0% per cm = 1.00 v/cm

CMOD and LPD – All Ranges 1.0 v = 1000 lb.

    Using load cell with x 10

    0.5%: 1 cm = 50 lb.
    1.0%: 1 cm = 100 lb.
    2.5%: 1 cm = 250 lb.
    5.0%: 1 cm = 500 lb.

Several load versus CMOD and LPD plots of typical beams are shown in Appendix II.

3.3 Testing Procedure

3.3.1 Testing of Precracked Beams

The maximum load calibration method (2, 3), which relates the load capacity of a concrete beam to the corresponding initial crack length as well as the initial compliance, was used for each precracked beam based on the three-point bend test. It is natural that the load capacity should decrease as the crack grows. As a result, a relationship could be found to predict other crack lengths.

Before precracking each beam, some preparation was needed. On the same day after casting, the specimens were removed from the curing room (i.e., the 30th day), and each beam was notched by a diamond saw at midspan to a depth of about 0.8" (20.3 mm). This was done to assure that the crack would start at midspan. At a week before the test, two aluminum sheets of 4"x 7.5" (102 mm x 191 mm) were attached using silicon rubber to either side of the specimen near the midspan to form a reservoir, as shown in Fig. 3.4.

Through the three-point bending test with strain control, each beam was loaded to a certain postpeak load on the softening branch, and then unloaded. At the same time, a plot of load versus CMOD was obtained. After this procedure, the dye (i.e., "Vanish", a product of the Drackett Products Company) was added into the reservoir, and

11

the beam specimen underwent a load-cycling procedure with a peak-load about one third of the load capacity, which lasted about 30 minutes. When the dye and the aluminum sheets were removed and the specimen was dried, a precracked beam was completed. This procedure is illustrated in Fig. 3.5 and referred to in Ref. 5. In Fig. 3.5(a), it is noted that the load with a scale of Y = 2.5 was removed after softening to a level about one half the peak load and the process restarted with Y = 1.0 (scale change only for convenience). Note that the crack closure effects (14) can be observed from the change of the initial slope in the restarted plot (Y = 1.0). Referring to the left curve in Fig. 3.5(b), a load-displacement plot is made for reference purposes. The load is then removed.

Once prepared (precracked) for testing, the beam was reloaded to failure, and the traces of P-CMOD and P-LPD were plotted at the same time. If a test to determine K_{IC} by the Jenq/Shah method (6) is required, for instance, it will be necessary to remove the load at 0.95 P_m on the unload curve and then reload to obtain the compliance at that load. This can be done even if load control is used.

After the beam was broken, the area of dyed surface was measured such that the initial, equivalent crack length could be calculated as:

$$a_i = \frac{\text{area of dyed surface}}{B}$$

12

The crack front surfaces for representative beams from each group with a_i/W about 0.5 are shown in Fig. 3.6.

For each group, the first eight beam specimens were used to obtain the relationships of the maximum load capacity P_m versus the initial crack length a_i, as well as versus the initial stiffness (i.e., the inverse of the initial compliance C_i) using the least squares method. Then the rest were tested based on the determined curve or equation to obtain a desired crack length by applying the load to a certain point. The calibration curves of P_m-a_i/W for different widths and curing conditions can be found in Figs. 3.7 to 3.9 and the compliance curves of P_m-$1/C_i$ for each group are shown in Figs. 3.10 to 3.15. Unfortunately, for both of the calibration curves of P_m-a_i/W for oven-dried beams, it was unsuccessful to apply the least squares method; however, a simple table could be set up instead by fitting the curves by eye. A table demonstrating these two curves is shown in Table 3.2.

3.3.2 Cylinder Tests

All of the properties of the concrete specimens were measured from the cylinder tests. The compressive strength fc', splitting-tensile strength ft', and the secant modulus of elasticity at 0.45 fc' were obtained from the tests in the conventional way. An additional experiment was made to measure the water content of the concrete specimens in different curing conditions. When the concrete specimen was

13

removed from the specific curing environment, one of the cylinders of the same batch as the specimen was taken out and weighed. After weighing, the cylinder was placed in an oven at a constant temperature of 105°C (221°F) 7 days (168 hrs) to drive the free water out and then the dried cylinder was weighed. The period of drying the cylinder was felt to be long enough and agreed with the work by Huang, Jiang and Best (15). The moisture content was therefore determined by dividing the free water by the dried weight of the cylinder. A summary of those results is shown in Tables 3.3 to 3.5.

3.4 Test Results and Comments

From Fig. 3.6, it is seen that the "side lips" are indeed a surface effect as the wider beams (series E) have a relatively flat crack front in the middle portion of the section in addition to the lips. Note that the oven-dried beams in both series (D1-D12, E1-E12) had connected and un-connected cracks near the surface of sufficient size to allow dye to penetrate in long, narrow zones, such as shown for beam D11. This is in contradistinction to a surface-penetration of 2-3 mm which occurred in most of the beams.

Because the "side lips" are a local phenomenon, it should be expected that the wider the beam, the closer the average crack depth a_i as determined here will be to the actual depth at the center "plateau". Hence, it may be expected that for a given load P_m, normalized to the beam width, the wider beams will have lower a_i than narrower

14

beams. This is indeed the case as is shown in Fig. 3.9 which displays a_i/W versus P_m for narrow (D) and wide (E) beams. If the curve for the wide beams is normalized to that for the narrow beams by dividing by two, it is seen that for the same load P_m the crack length of a wide beam is less than that of a narrow beam. For instance, compare the crack length of the wide beam at load 8 kN to that of the narrow beam at load 4 kN.

The tensile strength in Table 3.3 to 3.5 has two values which were obtained by using two different sizes of wood strips for the splitting test. Although the standard method of splitting test has been presented and applied for a long time, no manual or study mentioned details about the dimensions of wood strips for various sizes of cylinders. The standard width of the wood strip for the 6" x 12" (152 mm x 305 mm) cylinder specimen is 1 in. (25.4 mm). In the study, the width of the wood strip used was 1 in. and 0.5 in., and the corresponding tensile strengths of the concrete were denoted as f_{tw}' and f_{tn}', respectively. The tensile strengths tested using the wide strips were about 50% higher than those with narrow strips. It is felt more reasonable to used the narrow strip, proportioned to the standard size; however, the value obtained from using the wide strip seems closer to the value of modulus of rupture f_r', which is in an approximate range of 8 to $12 \sqrt{f_c'}$ in accordance to Reference (16).

Table 3.1 Mix Design

Water/Cement	0.49
Cement Type	I
S.G. Sand	2.65
S.G. Aggregate	2.56
S.G. Cement	3.15
% Sand by Weight	32.68
% Aggregate by Weight	47.46
% Cement by Weight	13.24
% Water by Weight	6.05
% Superplasticizer	0.44
Maximum aggregate size	0.75 in.(19 mm)

	lb/ft^3 (kg/m^3)	ft^3 (m^3)
Aggregate	71.05 (1138.0)	0.4448
Sand	48.92 (783.7)	0.2958
Cement	19.82 (317.5)	0.1008
Water	9.05 (145.0)	0.1450
Superplasticizer (S.G. = 2.0)	0.66 (10.6)	0.0053
Air		0.0083
Slump	1.00 in (25.4 mm)	

Unit Weight of Concrete = 149.5 lb/ft^3 (2395 kg/m^3)

Table 3.2 Data of P_m Versus a_i/W for Oven-Dried Beams

| P_m, | | a_i / W | |
kN	(lb)	(a) Narrow Beams	(b) Wide Beams
0.0	(0)	1.000	1.000
0.5	(112)	0.702	0.783
1.0	(225)	0.575	0.655
1.5	(337)	0.495	0.555
2.0	(449)	0.435	0.489
2.5	(562)	0.388	0.444
3.0	(674)	0.353	0.407
3.5	(787)	0.322	0.376
4.0	(899)	0.298	0.347
4.5	(1011)	0.278	0.325
5.0	(1124)	0.260	0.305
5.5	(1236)	0.246	0.288
6.0	(1348)	0.233	0.273
6.5	(1461)	0.224	0.260
7.0	(1573)	0.214	0.248
7.5	(1685)	0.206	0.239
8.0	(1798)	0.200	0.231
8.5	(1910)	0.194	0.224
9.0	(2022)	0.189	0.218
9.5	(2135)	0.185	0.212
10.0	(2247)	0.181	0.206
10.5	(2360)	0.178	0.200
11.0	(2472)	0.175	0.196

Note: This table refers to Fig. 3.7.

Table 3.3 Summary of The Oven-Dried Cylinder Data

	$^1f_c{'}$, psi MPa	$f_{tw}{'}$, psi MPa	$f_{tn}{'}$, psi MPa	E_c, psi×10^6 GPa	ϵ_0, in/in,×10^{-3} m/m,×10^{-3}	w, %
	7397 51.0	799 5.51	552 3.80	4.27 29.4	2.74	0.13
	8703 60.0	955 6.58	630 4.34	5.08 35.0	2.22	0.10
	9213 63.5	955 6.58	679 4.68	4.95 34.1	2.81	0.18
	7595 52.3	771 5.31	584 4.02	4.17 28.7	2.90	0.12
	6719 46.3	821 5.66	531 3.66	4.77 32.9	2.15	0.06
	7793 53.7	884 5.82	573 3.95	4.51 31.1	2.21	0.19
	7166 49.4	806 5.55	552 3.80	4.98 34.3	2.02	0.06
	8251 56.8	1016 7.00	601 4.13	5.06 34.9	1.81	0.12
	8581 59.1	828 5.70	523 3.60	5.09 35.1	2.22	0.06
	9250 63.7	817 5.63	587 4.04	4.76 32.8	2.26	0.12
N	29	10	10	10	10	10
Average	8067 55.6	865 5.96	581 4.00	4.76 32.8	2.33	0.11
Std Dev.	824 5.68	79 0.54	45 0.31	0.32 2.2	0.36	0.04
C. V.	10.2%	9.1%	7.7%	6.8%	15.5%	38.6%

[1] Average for each batch

18

Table 3.4 Summary of The Air-Dried Cylinder Data

	$^1f_c{}'$, psi MPa	$f_{tw}{}'$, psi MPa	$f_{tn}{}'$, psi MPa	E_c, psi$\times10^6$ GPa	ε_0, in/in,$\times10^{-3}$ m/m,$\times10^{-3}$	w, %
	8289 57.1	856 5.90	693 4.77	5.79 39.9	2.15	2.48
	9095 62.7	835 5.75	559 3.85	5.34 36.8	2.18	2.77
	9703 66.9	877 6.04	630 4.34	5.54 38.2	2.30	2.98
	9137 63.0	1004 6.92	707 4.87	5.38 37.1	2.10	2.32
	9887 68.1	1174 8.09	608 4.19	5.38 37.1	2.26	2.39
	10057 69.3	1125 7.75	622 4.29	5.42 37.3	2.14	2.43
	10254 70.7	1047 7.21	693 4.77	6.64 45.8	1.73	2.27
	9463 65.2	1075 7.41	736 5.07	5.53 38.1	2.04	2.43
	9887 68.1	923 6.36	736 5.07	6.34 43.7	2.22	2.82
	10099 69.9	1004 6.92	686 4.73	6.55 45.1	2.02	2.31
N	20	10	10	10	10	10
Average	9587 66.1	992 6.83	667 4.60	5.79 39.9	2.11	2.52
Std Dev.	572 3.94	111 0.76	56 0.39	0.49 3.38	0.16	0.23
C.V.	6.0%	11.2%	8.4%	8.5%	7.6%	9.3%

[1] average for each batch

Table 3.5 Summary of The Saturated Cylinder Data

	$^1f_c{}'$, psi MPa	$f_{tw}{}'$, psi MPa	$f_{tn}{}'$, psi MPa	E_c, psi$\times 10^6$ GPa	ϵ_0, in/in, $\times 10^{-3}$ m/m, $\times 10^{-3}$	w, %
	8769	905	619	5.06	1.73	3.78
	60.4	6.24	4.26	34.9		
	8161	983	559	5.40	1.98	3.88
	56.2	6.77	3.85	37.2		
	8359	898	615	5.54	1.80	3.27
	57.6	6.81	4.24	38.2		
	8529	912	559	5.80	2.17	4.03
	58.8	6.28	3.85	40.0		
	8670	1146	644	5.75	1.78	3.92
	59.7	7.90	4.44	39.6		
	7780	934	729	5.37	2.20	3.71
	53.6	6.44	5.02	37.0		
	8628	994	707	5.11	2.03	3.81
	59.4	6.85	4.87	35.2		
	8529	856	481	6.15	2.01	3.86
	58.8	5.90	3.31	42.4		
	8755	1082	601	5.82	1.96	3.61
	60.3	7.45	4.14	40.1		
	9151	927	644	5.61	2.13	3.62
	63.1	6.39	4.44	38.7		
N	26	10	10	10	10	10
Average	8529	964	616	5.56	1.98	3.75
	58.8	6.64	4.24	38.3		
Std Dev.	327	85	69	0.32	0.17	0.20
	2.25	0.59	0.48	2.20		
C.V.	3.8%	8.8%	11.2%	5.8%	9.6%	5.3%

^{1} average for each batch

Fig. 3.1 Test Setup for 8" Deep Beams (2)

21
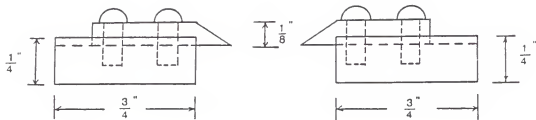
Side view
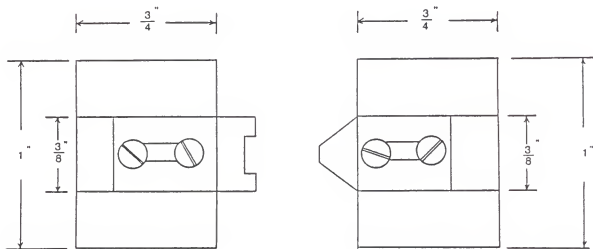
Plan view

1 in. = 25.4 mm

Fig. 3.2 A Set of Knife Edges for TPB Specimens
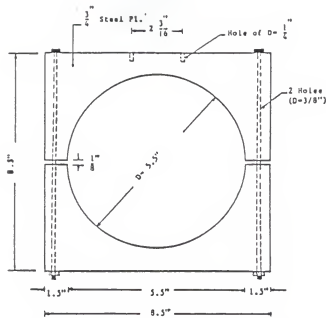
(a) Square Plate with a Circular Hole
(Attached to The Piston)
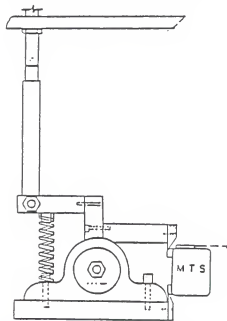
(b) Transducer-Supporting Device
(Attached to The Plate)

1 in. = 25.4 mm

Fig. 3.3 The LPD-Transducer Setup (2)

23
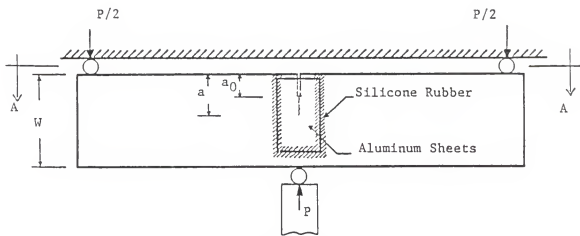
Elevation View
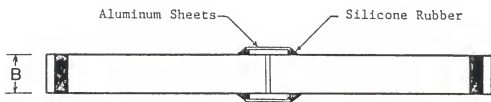
Section A-A View

Fig. **3.4** Details of The Dye Reservoir
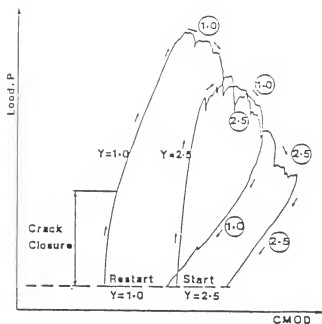
a. Precracking Process—
   Dye Not Applied
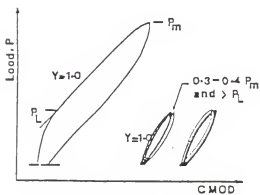
b. Load- Cycling
   With Dye Applied

Fig. 3.5 Specimen Precracking
        and Dye Application (5)

Dye

$$\frac{a_i}{W} = 0.52$$

D11, Oven

$$\frac{a_i}{W} = 0.50$$

D23, Air

$$\frac{a_i}{W} = 0.48$$

D36, Saturated

Dye

$$\frac{a_i}{W} = 0.50$$

E6, Oven

$$\frac{a_i}{W} = 0.50$$

E18, Air

$$\frac{a_i}{W} = 0.51$$

E29, Saturated
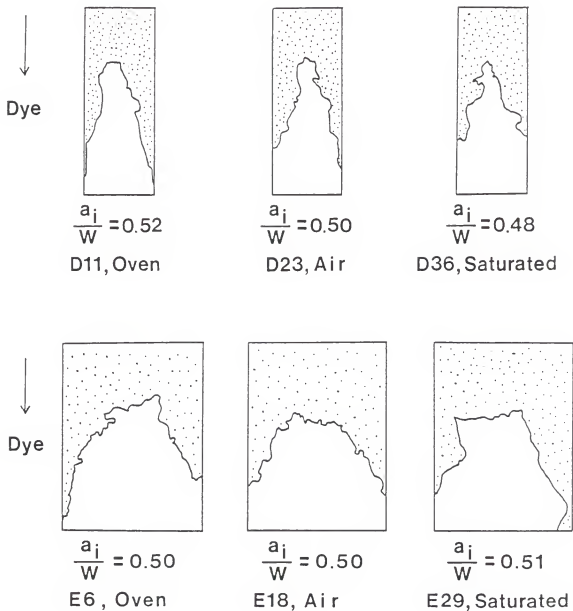
Fig. 3.6 The Typical Failure Surfaces for Each Group
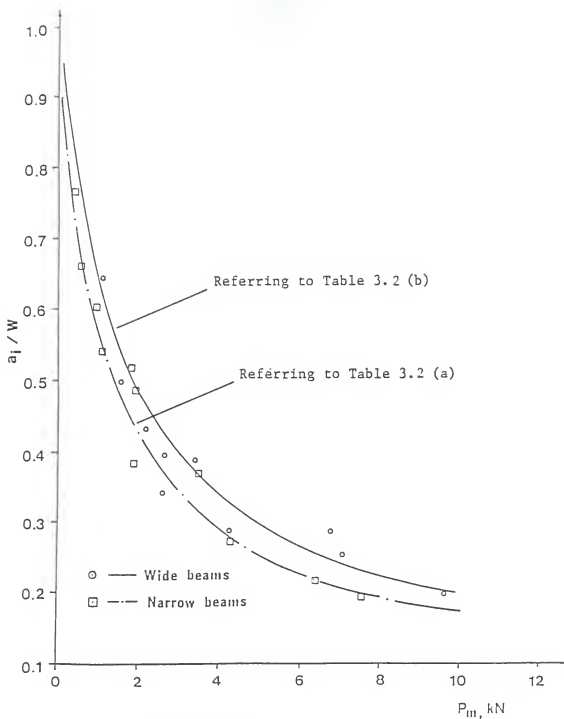
1 kN = 224.72 lb

Fig. 3.7 The Maximum Load Calibration Curves
for Oven-Dried Beams

$$\frac{a_i}{W} = 0.985 - 0.102\, P_m + 0.00390\, P_m^2$$

$$\frac{a_i}{W} = 0.945 - 0.181\, P_m + 0.00987\, P_m^2$$

Wide beams

Narrow beams

a_i / W

P_m, kN
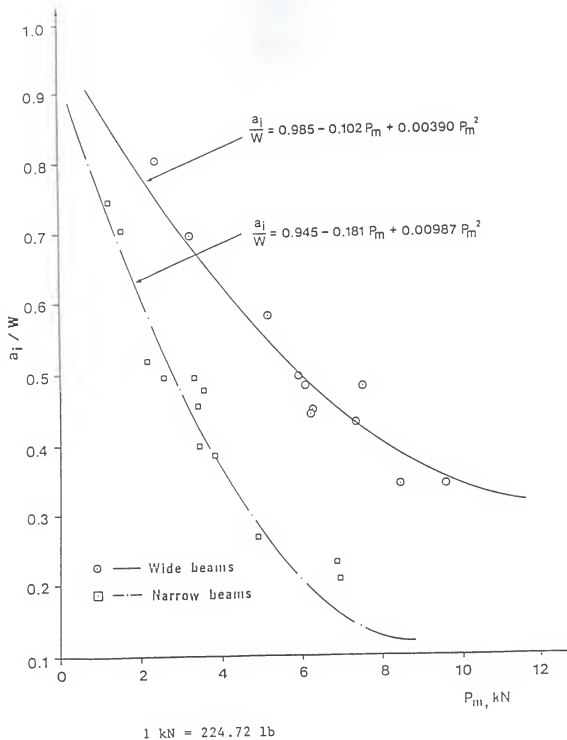
1 kN = 224.72 lb

Fig. 3.8 The Maximum Load Calibration Curves
for Air-Dried Beams

28

The equations shown on the figure:

$$\frac{a_i}{W} = 1.0 - 0.110 P_m + 0.00459 P_m^2$$

$$\frac{a_i}{W} = 1.0 - 0.144 P_m + 0.00631 P_m^2$$

Legend:

⊙ —— Wide beams
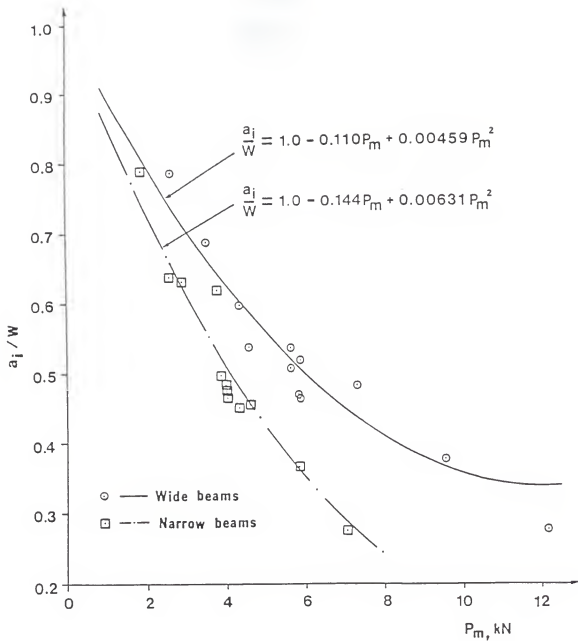
▢ —·— Narrow beams

1 kN = 224.72 lb

Fig. 3.9 The Maximum Load Calibration Curves
for Saturated Beams

The curve is labeled with the equation:

$$\frac{1}{C_i} = 3721 + 4662\,P_m + 241\,P_m^{\ 2}$$

Y-axis: $1\,/\,Ci$, $kN\,/\,m \times 10^4$

X-axis: P_m, kN
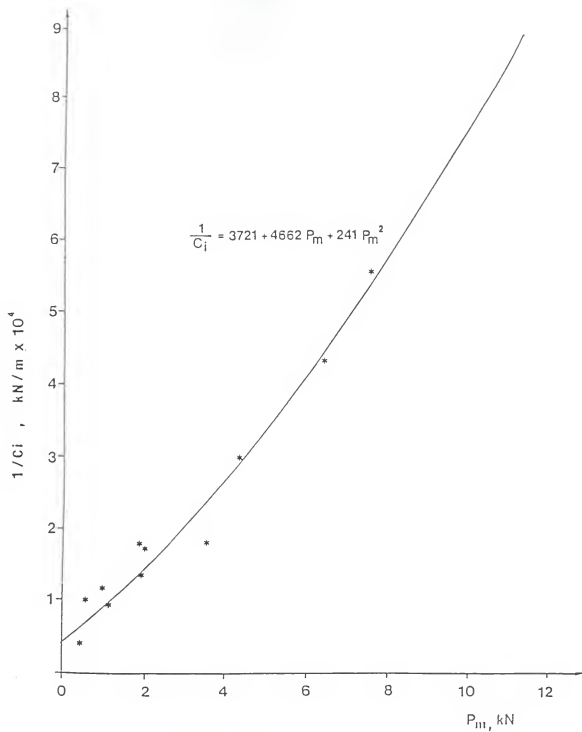
1 kN = 224.72 lb
1 kN/m = 5.708 lb/in

Fig. 3.10 The Compliance Calibration Curve
for Oven-Dried, Narrow Beams

30

$$\frac{1}{C_i} = 488 + 8998.5 \, P_m - 327.16 \, P_m^2$$

1 kN = 224.72 lb
1 kN/m = 5.708 lb/in
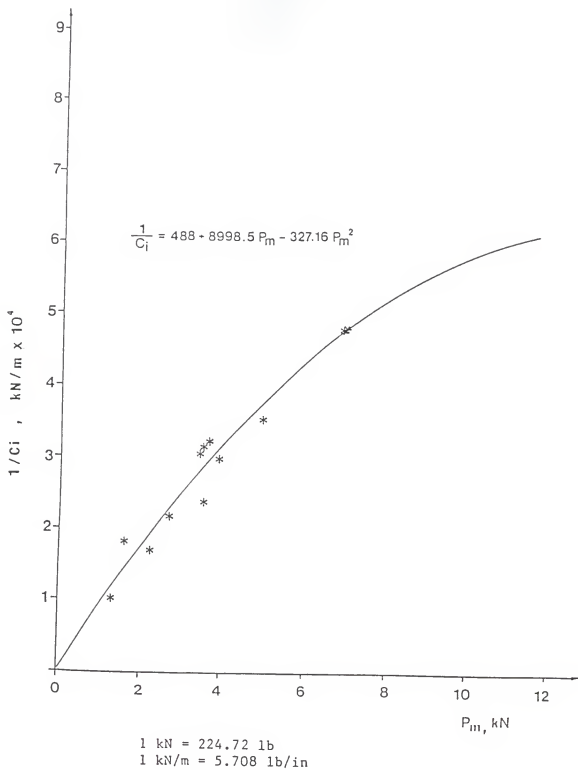
Fig. 3.11 The Compliance Calibration Curve
for Oven-Dried, Wide Beams

31

$$\frac{1}{C_i} = -1264 + 13690\, P_m - 937.79\, P_m^2$$

1 kN = 224.72 lb
1 kN/m = 5.708 lb/in
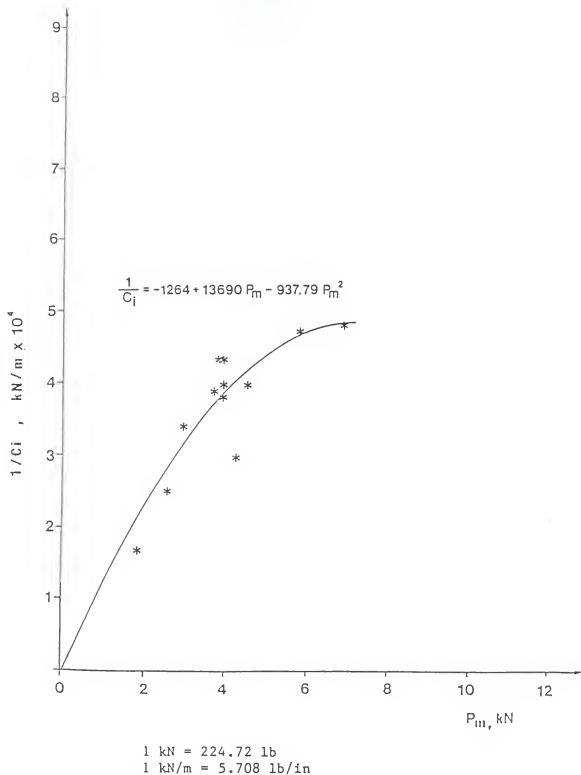
Fig. 3.12 The Compliance Calibration Curve
for Air-Dried, Narrow Beams

32

$$\frac{1}{C_i} = -2305 + 10499\,P_m - 328.85\,P_m^2$$
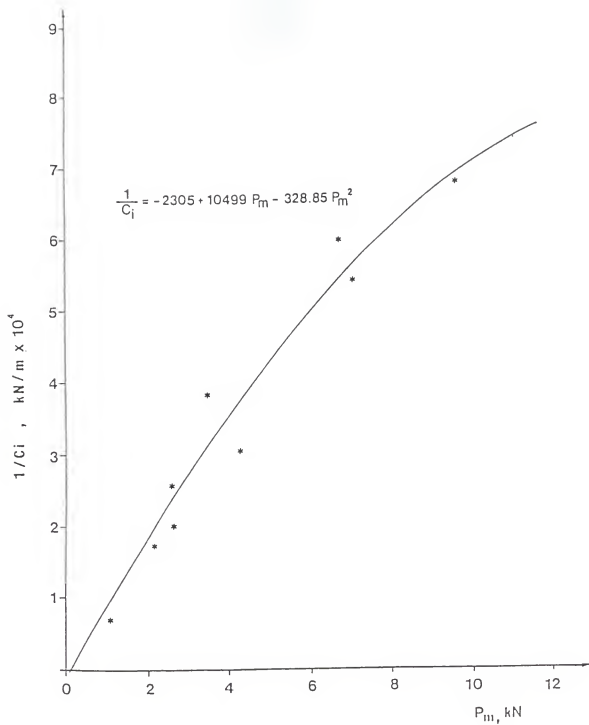
1 kN = 224.72 lb
1 kN/m = 5.708 lb/in

Fig. 3.13 The Compliance Calibration Curve
for Air-Dried, Wide Beams

33

$$\frac{1}{C_i} = 3013 + 6480.7\, P_m - 64.80\, P_m^2$$
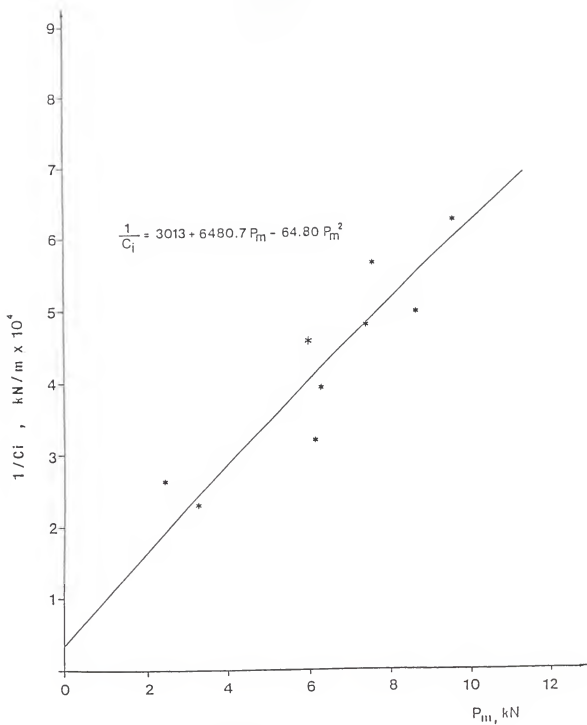
1 kN = 224.72 lb
1 kN/m = 5.708 lb/in

Fig. 3.14 The Compliance Calibration Curve
for Saturated, Narrow Beams

34

$$\frac{1}{C_i} = 91.33 + 9377.2 \, P_m - 319.18 \, P_m^2$$
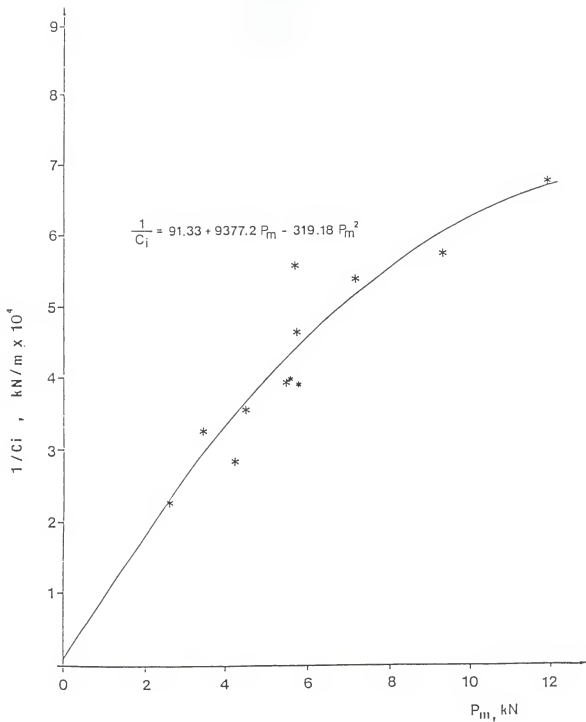
Fig. 3.15 The Compliance Calibration Curve
for Saturated, Wide Beams

1 kN = 224.72 lb
1 kN/m = 5.708 lb/in

35

CHAPTER 4

Applied Methods And Experimental Results

4.1   Methods of Calculation for Fracture Toughness

In the past decade, many researchers have conducted numerous experiments to develop approaches for estimating the critical stress intensity factor of cementious materials such as concrete. Some of those based on LEFM are proposed as standardized testing methods and presented herein along with other methods.

4.1.1 Go/Refai/Swartz (G/R/S) Method (1, 2, 3)

The formula used in this method is based on the bending analogy, and is similar to the Srawley formula (17). The Williams' stress function

$$\Phi = \sum_{n=1}^{N} r^{\frac{n+2}{2}} \left\{ a_n \left[\sin\left(\frac{n}{2} - 1\right)\theta - \frac{n-1}{n+2} \sin\left(\frac{n}{2} + 1\right)\theta \right] \right.$$

$$\left. + b_n \left[\cos\left(\frac{n}{2} - 1\right)\theta - \cos\left(\frac{n}{2} + 1\right)\theta \right] \right\} \quad ...(4.1)$$

was applied to the single-edge-notch beam and evaluated at 23 boundary stations, using the boundary collocation method. The first constant of those obtained by this method a_1, dominates the equation and is used to evaluate the stress intensity K_I since

$$K_I = -a_1 \sqrt{2\pi} \quad . \quad . \quad . \quad . \quad . \quad . \quad . \quad . \quad . \quad . \quad . \quad . \quad . \quad (4.2)$$

Then, through the use of the least squares method to curve-fit the numerical results, K_I could be estimated, using the following equation:

$$K_I = (M/BW^{1.5}) A(z), \qquad . \qquad . \qquad . \qquad . \qquad (4.3)$$

where $M = P_m S/4$

and, for $S/W = 4$

$$A(Z) = 1.503Z^2 - 6.989Z + 2.630 + 4.835Z^{-1} + 0.207Z^{-2}$$

$$Z = 1 - a/W$$

Coefficients of the function $A(Z)$ for other S/W ratios can be found in Reference (9).

To get the critical stress intensity factor K_{IC}, which is associated with the onset and continuation of unstable crack growth, the crack length must be used at the point of instability which lies on the descending portion of the P-CMOD curve with the value of $0.95P_m$. This crack length is called the effective crack length, a_e, in which the LEFM formula may still be used even when a process zone exists. By means of the maximum load calibration curve or equations given in Figs. 3.7 to 3.9, the effective crack length a_e can be easily found. After that, the value of K_{IC} can be calculated by substituting a_e into Equation (4.3).

Then, using the calculated K_{IC} the energy release rate based upon its LEFM definition can be obtained from the formula as:

$$G_{IC} = K_{IC}^2/E_c \quad . \quad . \quad . \quad . \quad . \quad . \quad . \quad . \quad . \quad . \quad . \quad . \quad . \quad . \quad (4.4)$$

In this, the effect of Poisson's ratio is neglected.

The average values of K_{IC} and G_{IC} for each beam series

with various curing conditions are shown in Tables 4.1 to 4.6, respectively, and a summary considering only $a_e/W \leq$ 0.65 (2, 3) is shown in Table 4.7. The effect of the three curing conditions for each beam series on K_{IC} is displayed in Figs. 4.1 and 4.2. Note that for both beam series the fracture toughness, K_{IC}, in air-dried and saturated conditions exhibits invariant values with the crack growth; while for the oven-dried beams a striking trend appears to occur: the K_{IC} values vary with the increase of the crack length. In addition, a plot of average K_{IC} versus moisture content is shown in Fig. 4.3. It is seen that the average values of K_{IC} for oven-dried beams are very low as compared with either those for air-dried or saturated.

4.1.2   Jenq/Shah (J/S) Method (6)

On the basis of LEFM and nonlinear fracture mechanics, a two-parameter model (i.e., $K_{IC}^{s} = K_{IC}$ and $CTOD_c$) is suggested to characterize the fracture process of concrete. In this study, the critical tip opening displacement, $CTOD_c$ was not determined. The concept behind this model can be explained from the P versus CMOD relationship. Initially, the P-CMOD plot is linear up to about half the maximum load while the corresponding crack tip opening displacement, CTOD, is zero. Then, a significant inelastic displacement and slow crack growth occur during which the load increases from 0.5 P_m on the ascending part to 0.95 P_m on the descending branch. The latter load station defines the

critical point, often called the point of instability, in which the CTOD, as well as K_I, reaches a critical value, i.e., CTOD = $CTOD_c$ and $K_I = K_{IC}$.

To calculate the stress intensity factor, the effective crack length a_e should be determined first. Before using the proposed equation by this method, an initial crack length a_i must be measured experimentally or obtained as a function of Young's Modulus E_t and the initial compliance C_i:

$$E_t = 6S \ (a_i + HO)(1/C_i) \ V_1(A)/W^2 B, \quad . \quad . \quad . \quad . \quad (4.5)$$

in which, HO is the distance from the face of the beam to the knife edge to which the transducer is attached. The term $V_1(A)$ is defined as

$$V_1(A) = 0.76 - 2.28A + 3.87A^2 - 2.04A^3 + 0.66/(1-A)^2. (4.6)$$

and $A = a_i / W$.

Knowing a_i and the unloading compliance C_u at 0.95 P_m, a trial and error method or numerical iteration scheme can be applied to determine the effective crack length a_e by satisfying the following equation.

$$E_t = 6S \ (a_e + HO)(1/C_u) \ V_1(a_e/W) \ /W^2 B \quad . \quad . \quad . \quad (4.7)$$

where E_t is the same as in Equation (4.5).

Herein, the Newton's Method is utilized to obtain the effective crack length a_e. First, equate Equations (4.6) to (4.7) so that the terms of E_t, S, W, B can be canceled out. Then

$$(\ a_e \ + \ HO \ ) \ V_1(\frac{a_e}{W}) = \frac{C_u}{C_i} \ (\ a_i \ + \ HO \ ) \ V_1 (\ A \ ) \ ... \ (4.8)$$

Since HO, C_u and C_i are known, and the initial crack length a_i is experimentally determined, a constant value can be created on the right-hand side of Equation (4.8). Then, after proceeding through an iteration process, the only variable a_e can be obtained.

Once a_e is obtained, the critical stress intensity factor as well as the critical energy release rate are calculated applying Go's formula, i.e., Equations (4.3) and (4.4). The results in Tables 4.8 and 4.9 are for those beams for which unloading data were taken.

4.1.3 The Karihaloo/Nallathambi (K/N) Method (7)

Karihaloo and Nallathambi proposed an analytical expression for determining K_c and G_c of a three-point bend concrete beam. In this method, the extended crack growth is based on the results of a series of tests and a self-consistent approximation to the nonlinear response of slow crack growth prior to fracture. At the growing crack front, the Young's Modulus E_e is reduced and depends not only on the mix variables, but also on the specimen dimensions and geometry. A regression formula based on this concept using a finite element method and various experimental results is used to estimate the extended crack length as follows:

$$(a_e - a)/W = \frac{f_c{'}}{E_c} [\beta_0 + \beta_1 (\frac{g}{g+1})^2 + \beta_2 (\frac{g}{g+1}) (\frac{a}{W})$$
$$+ \beta_3 (\frac{a}{W}) (\frac{S}{W}) + \beta_4 (\frac{W}{W+1})] \ . \ . \ . \ . \ . \ (4.9)$$

40

where the regression coefficients are

$\beta_o = 3960$

$\beta_1 = 144$

$\beta_2 = -88.2$

$\beta_3 = 8.7$

$\beta_4 = -3950$

In Equation (4.9), the crack length $a = a_{0i}$ for precracked beams. The maximum aggregate size, g used herein, is 0.75 in. (19 mm) for all concrete specimens.

After the extended crack length is found, the stress intensity factors and the energy release rate at the tip of an advancing crack can be calculated from the following formulas:

$$K_{IC} = \sigma_0 \ a_e \ y_1 \ (a_e/W) \ y_2 \ (a_e/W \ , \ S/W) \quad . \quad . \quad . \ (4.10)$$

$$G_{IC} = (\sigma_0^2 \ a_e \ / \ E_c) \ z_1 \ (a_e \ /W) \ z_2 \ (a_e \ /W, \ S/W) .. (4.11)$$

$$\sigma_0 = 1.5 \ PS/BW^2 \quad . \quad . \quad . \quad . \quad . \quad . \quad . \quad . \quad . \quad . \ (4.12)$$

The various functions appearing in Equations (4.10) and (4.11) are defined as follows:

$$y_1(a_e/W) = A_0 + A_1 \ (a_e/W) + A_2 \ (a_e/W)^2 + A_3(a_e/W)^3 + A_4 \ (a_e/W)^4$$

$$y_2 \ (a_e/W \ , \ S/W) = B_0 + B_1 \ (S/W) + B_2 \ (S/W)^2 + B_3 \ (S/W)^3$$
$$+ B_4 \ (S/W) \ (a_e/W) + B_5 \ (S/W)^2(a_e/W)$$

$$z_1(a_e/W) = C_0 + C_1(a_e/W) + C_2(a_e/W)^2 + C_3 \ (a_e/W)^3 + C_4(a_e/W)^4$$

$$z_2 \ (a_e/W \ , \ S/W) = D_0 + D_1 \ (S/W) + D_2 \ (S/W)^2 + D_3 \ (S/W)^3$$
$$+ D_4 \ (S/W) \ (a_e/W) + D_5 \ (S/W)^2(a_e/W)$$

The coefficients A_i, B_i, C_i, D_i are given in the following table.

i	Ai	Bi	Ci	Di
0	3.646	0.4607	1.564	1.9560
1	-6.789	0.0484	-8.32	0.3982
2	39.240	-0.0063	52.95	-0.0553
3	-76.820	0.0003	-124.9	0.0027
4	74.330	-0.0059	122.9	0.0202
5	----	0.0003	----	-0.0055

In order to apply this method to the precracked beams, the initial crack depth was assumed to be outside the process zone, i.e., excluding any microcracking, and was equal to a_{oi}, the distance from the crack "mouth" to the root of the "V-shape" revealed by the dye. The results obtained from several specific beams are shown in Tables 4.10 and 4.11.

4.2   Methods of Calculation for Energy Release Rate

The methods for determining the energy release rate mentioned in Section 4.1 are based on the determined stress intensity using LEFM and represent only the surface energy of separation. Since a process (plastic) zone exists in the fracture of real concrete, these energy release rates determined from the above methods are not representative. Instead of this, some other approaches are proposed to obtain more realistic values of energy release rates. Two of them are presented herein:

4.2.1   J-Integral Method

This method uses the concept of the J-Integral developed by Rice (10), who defined a number of applicable contour integrals which are path-independent by virtue of the theorem of energy conservation. This method was adapted by Go (4) in a statistical approach. The J-Integral along a contour around the crack tip is considered to be the change in potential energy for a virtual crack extension

$$dV = - J \, da \qquad . \quad . \quad . \quad . \quad . \quad . \quad . \quad (4.13)$$

where V is the potential energy.

Go proposed a formula that determines the energy release rate directly by the change in energy versus the change in crack extension and also includes the surface roughness effect using a 15% increase in fracture area. To do this in a statistical sense, the energy data U, i.e., the area under load versus LPD curve from point of zero load to point of instability, is measured and plotted versus a/W where a may be the initial crack length a_i or the effective crack length a_e. The slope of the best line to fit those data gives the energy release rate as

$$J_{IC} = \frac{1}{1.15 \, BW} \left| \frac{dU}{d(a/W)} \right| \qquad . \quad . \quad . \quad . \quad (4.14)$$

The results for all the beams are shown in Tables 4.13 and 4.14, and in Figs. 4.4 to 4.6.

4.2.2 Energy Release Method (2, 5)

The basic feature of this method is based on the fundamental definition of the energy release rate G (18).

43

For a structure of unit thickness under the action of the load P, the load point undergoes a relative displacement v. When the crack increases in size by an amount da, the displacement will increase by an amount dv. Hence, the work done by the external force is Pdv. If the total elastic energy is U_t, then the energy release rate following (18) is

$$G = d(Pv-U_t) / da \qquad . \quad . \quad . \quad . \quad . \quad . \quad (4.15)$$

Use this concept, a formula was presented by Refai (5).

$$G_{IC} = \frac{1}{1.15BW} \left[\frac{P_i dv}{d(a/W)_i} - \frac{dU_i}{d(a/W)_i} \right] \quad . \quad . \quad . (4.16)$$

In this, the softening portion of the load versus LPD diagram is divided into many segments of the same width (i.e., dv is kept constant) as shown in Fig. 4.7. The width dv is selected depending on the accuracy required. P_i is the average load in the ith interval. The term $d(a/W)i$ represents the change in crack length versus beam depth in the ith interval; it can be found from the maximum load calibration curve or equation. The change of energy dU_i corresponds to the decrease in elastic energy due to the incremental crack growth at ith stage. It can be estimated by using the unloading slope which may be obtained from the curve or equation of maximum load versus compliance to measure the difference in triangular areas corresponding to the changes in the elastic energy.

This was done only for several selected beams which had nice traces in the P-LPD plots. The results from typical beams for each group are plotted in Fig.4.8 to 4.10.

4.3 Summary of the experimental results

1. From the tables for 3 in. and 6 in. beams, and neglecting the beams with $a_e/W > 0.65$, the average values of K_{IC} for air-dried beams are 803 lb-in$^{-3/2}$ (883 kN-m$^{-3/2}$) with C.V.= 2.8% and 876 lb-in$^{-3/2}$ (961 kN-m$^{-3/2}$) with C.V.= 2.0%, respectively, which shows no significant difference between them. Similar results for saturated beams with 3 in. and 6 in. wide are 1180 lb-in$^{-3/2}$ (1300 kN-m$^{-3/2}$) with C.V.= 2.1% and 860 lb-in$^{-3/2}$ (956 kN-m$^{-3/2}$) with C.V.= 7.3%, which implies a side (width) effect on them. In oven-dried condition, the average K_{IC} values are 559 lb-in$^{-3/2}$ (615 kN-m$^{-3/2}$) with C.V.= 36.2% for 3 in. wide beams and 361 lb-in$^{-3/2}$ (397 kN-m$^{-3/2}$) with C.V.= 32.9% for 6 in. wide beams. It is noted that the coefficients of variance for both the 3 in. and 6 in. wide oven-dried beams are very high compared to those in the air-dried and saturated conditions so that the average values for oven-dried beams are meaningless.

2. Results of the determination of K_{IC} from the J/S method and the K/N method based on some specific beams and compared with the G/R/S method are summarized in Table 4.12. It is seen that the results obtained from the G/R/S method and the J/S method seem to be more consistent in value; while the K/N method turn out higher values than those from the previous methods. However, basically, the results from the three methods are in agreement.

3. The energy release rate J_{IC} as determined from the plots for both the 3 in. and 6 in. wide beams are

45

respectively, 0.274 lb/in (47.9 N/m) and 0.184 lb/in (32.2 N/m) in the oven-dried condition; 0.222 lb/in (38.9 N/m) and 0.239 lb/in (41.9 N/m) in the air-dried condition; 0.268 lb/in (47.0 N/m) and 0.285 lb/in (49.9 N/m) in the saturated condition. These values are higher than those of the average G_{IC} based on calculated K_{IC} by the Go/ Refai/Swartz method as given in Table 4.7.

4. Each point in Fig 4.8 to 4.10 denotes the corresponding G_{IC} value to each ith segment of any typical beam, selected from a certain group. To some extent, G_{IC} is constant with an average of 0.261 lb/in (45.7 N/m) for air-dried, narrow beam D23; the others display a striking trend, and it is not meaningful to find average values.

Table 4.1 K_{IC} Data by G/R/S Method for Oven-Dried Narrow Beams

No.	a_i/W	a_i/W^*	a_e/W^*	P_m lb kN	K_{IC} lb-in$^{-3/2}$ kN-m$^{-3/2}$	G_{IC} lb/in N/m
D1	0.195	0.205	0.210	1720	912	0.175
				765	1003	30.61
D2	0.219	0.223	0.230	1460	820	0.141
				650	902	24.77
D3	0.273	0.283	0.292	980	656	0.090
				436	721	15.82
D4	0.367	0.320	0.329	800	592	0.074
				356	651	12.91
D5	0.381	0.445	0.455	430	448	0.042
				191	492	7.38
D6	0.539	0.555	0.560	255	358	0.027
				113	393	4.71
D7	0.602	0.580	0.590	220	338	0.024
				98	372	4.21
D8	0.660	0.670	0.675	135	276	0.016
				60	304	2.81
D9	0.766	0.720	0.735	100	260	0.014
				45	286	2.49
D10						
D11	0.518	0.450	0.459	420	442	0.041
				187	486	7.20
D12	0.489	0.435	0.457	445	466	0.046
				198	512	7.99
				Avg.	506	0.063
					557	10.99
				C.V.	40.7%	80.6%

* Value from the fitting curve.

Table 4.2 K_{IC} Data by G/R/S Method for Air-Dried Narrow Beams

No.	a_i/W	a_i/W^*	a_e/W^*	P_m lb kN	K_{IC} lb-in$^{-3/2}$ kN-m$^{-3/2}$	G_{IC} lb/in N/m
D13	0.208	0.160	0.175	1600	764	0.101
				712	840	17.66
D14	0.269	0.288	0.307	1130	788	0.107
				503	867	18.78
D15	0.743	0.722	0.732	300	770	0.102
				134	847	17.96
D16	0.497	0.521	0.542	615	818	0.116
				274	900	20.25
D17	0.399	0.423	0.442	810	814	0.114
				360	895	20.05
D18	0.703	0.679	0.690	365	790	0.108
				162	869	18.87
D19	0.234	0.164	0.179	1580	764	0.101
				703	840	17.65
D20	0.520	0.588	0.604	510	819	0.116
				227	901	20.30
D21	0.385	0.382	0.407	890	814	0.114
				396	895	20.03
D22	0.456	0.427	0.448	800	817	0.115
				356	899	20.21
D23	0.497	0.438	0.458	780	819	0.116
				347	901	20.29
D24	0.478	0.410	0.431	835	814	0.115
				372	896	20.07
				Avg.	799	0.110
					879	19.34
				C.V.	2.72%	5.40%

* Value from the fitting curve.

Table 4.3 K_{IC} Data by G/R/S Method for Saturated Narrow Beams

No.	a_i/W	a_i/W^*	a_e/W^*	P_m lb kN	K_{IC} lb-in$^{-3/2}$ kN-m$^{-3/2}$	G_{IC} lb/in N/m
D25	0.273	0.293	0.315	1580 703	1126 1239	0.228 39.95
D26	0.636	0.665	0.679	580 258	1204 1324	0.261 45.67
D27	0.457	0.468	0.487	1030 458	1172 1289	0.247 43.25
D28	0.788	0.748	0.758	420 187	1215 1336	0.265 46.49
D29	0.630	0.628	0.644	660 294	1209 1330	0.263 46.08
D30	0.366	0.366	0.386	1325 590	1144 1259	0.236 41.27
D31	0.618	0.542	0.558	850 378	1185 1304	0.253 44.27
D32	0.451	0.490	0.509	970 432	1174 1291	0.248 43.40
D33	0.475	0.521	0.540	900 401	1190 1309	0.255 44.64
D34	0.494	0.530	0.550	874 389	1190 1309	0.255 44.64
D35	0.464	0.521	0.540	900 401	1190 1309	0.255 44.64
D36	0.483	0.521	0.540	900 401	1190 1309	0.255 44.64
				Avg.	1183 1301	0.252 44.08
				C.V.	2.09%	4.10%

* Value From the fitting curve.

Table 4.4 K_{IC} Data by G/R/S Method for Oven-Dried Wide
Beams

No.	a_i/W	a_i/W^*	a_e/W^*	P_m lb kN	K_{IC} lb-in$^{-3/2}$ kN-m$^{-3/2}$	G_{IC} lb/in N/m
E1	0.204	0.208	0.214	2200	590	0.073
				979	649	12.81
E2	0.291	0.258	0.258	1550	472	0.047
				690	519	8.19
E3	0.258	0.245	0.252	1620	485	0.049
				721	533	8.65
E4	0.291	0.330	0.340	980	374	0.029
				436	411	5.14
E5	0.391	0.375	0.385	780	336	0.024
				347	370	4.15
E6	0.499	0.540	0.550	360	245	0.013
				160	270	2.21
E7	0.432	0.465	0.475	500	275	0.016
				223	303	2.78
E8	0.647	0.625	0.640	255	230	0.011
				113	253	1.95
E9	0.397	0.428	0.437	610	302	0.019
				271	333	3.37
E10						
E11						
E12	0.342	0.430	0.440	600	300	0.019
				267	330	3.31
				Avg.	361	0.030
					397	5.26
				C.V.	31.1%	63.5%

* Value from the fitting curve.

Table 4.5 K_{IC} Data by G/R/S Method for Air-Dried Wide Beams

No.	a_i/W	a_i/W^*	a_e/W^*	P_m lb kN	K_{IC} lb-in$^{-3/2}$ kN-m$^{-3/2}$	G_{IC} lb/in N/m
E13	0.345	0.391	0.406	1950	889	0.136
				868	978	23.90
E14	0.444	0.489	0.505	1440	861	0.128
				641	947	22.45
E15	0.698	0.685	0.696	760	841	0.122
				338	925	21.42
E16	0.585	0.549	0.566	1200	857	0.127
				534	943	22.22
E17	0.345	0.356	0.371	2200	912	0.144
				979	1004	25.19
E18	0.500	0.503	0.523	1375	866	0.129
				612	952	22.68
E19	0.805	0.750	0.761	570	836	0.121
				254	920	21.16
E20	0.487	0.427	0.443	1740	877	0.133
				774	964	23.26
E21	0.439	0.436	0.452	1700	878	0.133
				757	966	23.32
E22	0.450	0.487	0.502	1450	860	0.128
				645	946	22.38
E23	0.485	0.493	0.511	1420	864	0.129
				632	950	22.58
E24						
				Avg.	867	0.130
					954	22.78
				C.V.	2.35%	4.72%

* Value from the fitting curve.

Table 4.6 K_{IC} Data by G/R/S Method for Saturated Wide Beams

No.	a_i/W	a_i/W^*	a_e/W^*	P_m lb kN	K_{IC} lb-in$^{-3/2}$ kN-m$^{-3/2}$	G_{IC} lb/in N/m
E25	0.373	0.364	0.375	2140	897	0.140
				950	987	24.53
E26	0.536	0.589	0.605	1025	826	0.123
				456	908	21.48
E27	0.684	0.663	0.676	790	811	0.118
				352	892	20.72
E28	0.482	0.435	0.450	1650	847	0.129
				754	932	22.63
E29	0.509	0.524	0.537	1270	833	0.125
				565	916	21.84
E30	0.594	0.607	0.623	970	828	0.123
				432	911	21.61
E31	0.786	0.735	0.748	595	821	0.121
				265	903	21.23
E32	0.277	0.335	0.336	2725	1028	0.190
				1213	1131	33.31
E33	0.534	0.520	0.537	1270	833	0.125
				565	916	21.84
E34	0.467	0.510	0.527	1310	834	0.125
				583	918	21.93
E35	0.465	0.508	0.525	1320	836	0.126
				587	919	22.01
E36	0.516	0.508	0.525	1320	836	0.126
				587	919	22.01
				Avg.	852	0.131
					938	22.93
				C.V.	6.64%	14.2%

* Value from the fitting curve.

Table 4.7 Average Value of Fracture Parameters

Curing Condition	Size Group No.	K_{IC}[1] lb-in$^{-3/2}$ kN-m$^{-3/2}$	G_{IC}[2] lb/in N/m	a_e/W Range
Oven-Dried	B = 3 in. D1-D12	559 615 [3]C.V.= 36.2 %	0.0656 11.5 N = 9	0.210-0.590
	B = 6 in. E1-E12	361 397 C.V.= 32.9 %	0.0274 4.8 N = 10	0.214-0.640
Air-Dried	B = 3 in. D13-D24	803 883 C.V.= 2.8 %	0.111 19.4 N = 10	0.175-0.604
	B = 6 in. E13-E24	874 961 C.V.= 2.0 %	0.250 23.1 N = 9	0.371-0.511
Saturated	B = 3 in. D25-D36	1180 1300 C.V.= 2.1 %	0.250 43.8 N = 11	0.315-0.644
	B = 6 in. E25-E36	860 946 C.V.= 7.3 %	0.133 23.3 N = 10	0.336-0.623

1. K_{IC} determined by Go/Refai/Swartz method (1, 2, 3), and $a_e/W \leq 0.65$.

2. $G_{IC} = K_{IC}^2 / E_c$.

3. The C.V. values calculated only for K_{IC} data.

Table 4.8 K_{IC} Data by Jenq/Shah Method (6) for Narrow Beams

No.	a_i/W	a_e/W	P_m lb kN	K_{IC} lb-in$^{-3/2}$ kN-m$^{-3/2}$	G_{IC} lb/in N/m
(Oven Dried)					
D11	0.518	0.594	420	654	0.090
			1.87	719	15.72
D12	0.489	0.531	445	573	0.069
			1.98	631	12.10
			Avg.	613	0.079
				675	13.91
(Air Dried)					
D21	0.385	0.422	890	847	0.124
			3.96	932	21.72
D22	0.456	0.478	800	888	0.136
			3.56	976	23.83
D23	0.497	0.550	780	1063	0.195
			3.47	1168	34.14
D24	0.478	0.539	835	1101	0.209
			3.72	1211	36.69
			Avg.	975	0.166
				1072	29.10
(Saturated)					
D33	0.475	0.527	900	1146	0.236
			4.01	1261	41.41
D34	0.494	0.517	874	1082	0.210
			3.89	1190	36.88
D35	0.464	0.498	900	1056	0.200
			4.01	1161	35.12
D36	0.483	0.510	900	1092	0.214
			4.01	1201	37.58
			Avg.	1094	0.215
				1203	37.74

Table 4.9 K_{IC} Data by Jenq/Shah Method (6) for Wide Beams

No.	a_i/W	a_e/W	P_m lb kN	K_{IC} lb-in$^{-3/2}$ kN-m$^{-3/2}$	G_{IC} lb/in N/m
(Oven Dried)					
E9	0.397	0.439	610	304	0.019
			2.71	334	3.40
E12	0.342	0.383	600	257	0.014
			2.67	283	2.43
			Avg.	281	0.017
				309	2.92
(Air Dried)					
E21	0.439	0.478	1700	943	0.154
			7.57	1037	26.91
E22	0.450	0.492	1450	836	0.121
			6.45	920	21.16
E23	0.485	0.533	1420	920	0.146
			6.32	1012	25.62
			Avg.	900	0.140
				990	24.56
(Saturated)					
E33	0.534	0.567	1270	910	0.149
			5.65	1001	26.08
E34	0.467	0.500	1310	773	0.107
			5.83	850	18.81
E35	0.465	0.506	1320	792	0.113
			5.87	871	19.76
E36	0.516	0.541	1320	875	0.138
			5.87	963	24.15
			Avg.	837	0.127
				921	22.20

Table 4.10 K_{IC} Data by Karihaloo/Nallathambi Method (7) for Narrow Beams

No.	a_{oi}/W	a_e/W	P_m lb kN	K_{IC} lb-in$^{-3/2}$ kN-m$^{-3/2}$	G_{IC} lb/in N/m
(Oven Dried)					
D11	0.293	0.538	420	688	0.092
			1.87	757	16.12
D12	0.238	0.487	445	614	0.074
			1.98	675	12.89
			Avg.	651	0.083
				716	14.51
(Air Dried)					
D21	0.231	0.476	890	1182	0.224
			3.96	1300	39.32
D22	0.281	0.521	800	1237	0.245
			3.56	1361	42.92
D23	0.269	0.510	780	1161	0.216
			3.47	1277	37.88
D24	0.281	0.521	835	1291	0.267
			3.72	1420	46.77
			Avg.	1218	0.238
				1340	41.72
(Saturated)					
D33	0.294	0.516	900	1365	0.311
			4.01	1501	54.44
D34	0.280	0.503	874	1269	0.269
			3.89	1395	47.09
D35	0.279	0.502	900	1302	0.283
			4.01	1432	49.63
D36	0.248	0.473	900	1187	0.236
			4.01	1305	41.28
			Avg.	1281	0.275
				1409	48.11

Table 4.11 K_{IC} Data by Karihaloo/Nallathambi Method (7) for Wide Beams

No.	a_{oi}/W	a_e/W	P_m lb kN	K_{IC} lb-in$^{-3/2}$ kN-m$^{-3/2}$	G_{IC} lb/in N/m
(Oven Dried)					
E9	0.250	0.498	610	436	0.037
			2.71	480	6.51
E12	0.175	0.430	600	346	0.024
			2.67	381	4.13
			Avg.	391	0.030
				430	5.32
(Air Dried)					
E21	0.313	0.551	1700	1459	0.340
			7.57	1605	59.49
E22	0.288	0.528	1450	1146	0.210
			6.45	1260	36.79
E23	0.363	0.597	1420	1453	0.331
			6.32	1598	58.02
			Avg.	1353	0.294
				1488	51.45
(Saturated)					
E33	0.363	0.580	1270	1215	0.243
			5.65	1336	42.56
E34	0.295	0.517	1310	996	0.166
			5.83	1096	29.02
E35	0.295	0.517	1320	1004	0.168
			5.87	1104	29.46
E36	0.355	0.572	1320	1227	0.249
			5.87	1350	43.56
			Avg.	1111	0.206
				1221	36.15

Table 4.12 Average Values of Fracture Toughness Using Three Methods

Curing Condition	Beam Nos.	K_{IC}, lb-in$^{-3/2}$ kN-m$^{-3/2}$		
		G/R/S[1]	J/S[2]	K/N[3]
Oven-Dried	D11, D12	454	613	651
		499	674	716
	E9, E12	300	270	391
		330	297	430
Air-dried	D21, D22,	816	975	1218
	D23, D24	898	1072	1340
	E21, E22,	867	855	1353
	E23	954	940	1488
Saturated	D33, D34,	1190	1094	1281
	D35, D36	1309	1203	1409
	E33, E34,	835	796	1110
	E35, E36	918	876	1221

1. Method of Go, Refai, Swartz (1, 2, 3)

2. Method of Jenq, Shah (6)

3. Method of Karihaloo, Nallathambi (7)

Table 4.13 J_{IC} Values for Narrow Beams (2, 4)

No.	a_i/W	U,lb-in			
(Oven-dried)					
D1	0.195	4.65			
D2	0.219	3.63			
D3	0.273	3.16			
D4	0.367	3.11			
D5	0.381	1.51			
D6	0.539	0.89			
D7	0.602	0.52			
D8	0.660	0.31	N = 11		
D9	0.766	0.32	Y = -7.55 X + 5.34		
D11	0.518	1.35	COR = -0.938		
D12	0.489	1.44	J_{IC} = 0.274 lb/in		
			(48.0 N/m)		
(Air-dried)					
D13	0.208	2.26			
D14	0.269	3.83			
D15	0.743	0.45			
D16	0.497	1.83			
D17	0.399	2.71			
D18	0.703	0.86			
D19	0.234	4.90			
D20	0.520	1.68			
D21	0.385	2.78	N = 12		
D22	0.456	2.14	Y = -6.12 X + 5.06		
D23	0.497	2.03	COR = -0.853		
D24	0.478	2.30	J_{IC} = 0.222 lb/in		
			(38.9 N/m)		
(Saturated)					
D25	0.273	5.00			
D26	0.636	1.50			
D27	0.457	2.71			
D28	0.788	0.99			
D29	0.630	1.35			
D30	0.366	4.05			
D31	0.618	1.94			
D32	0.451	2.91			
D33	0.475	1.89	N = 12		
D34	0.494	1.88	Y = -7.4 X + 6.15		
D35	0.464	2.01	COR = -0.878		
D36	0.483	2.15	J_{IC} = 0.268 lb/in		
			(47.0 N/m)		

Note: U = area under P-LPD from 0 to 0.95 P_m on
      the descending branch.

      1 lb-in = 0.113 N-m

Table 4.14 J_{IC} Values for Wide Beams (2, 4)

```
----------------------------------------------------------
No.         a_i/W      U,lb-in
----------------------------------------------------------
(Oven-dried)
E1          0.204       7.03
E2          0.291       4.90
E3          0.258       4.60
E4          0.291       3.26
E5          0.391       1.81
E7          0.432       1.52     N = 9
E8          0.647       2.07     Y = -10.16 X + 6.86
E9          0.397       1.95     COR = -0.681
E12         0.342       1.54     J_IC = 0.184 lb/in
                                      ( 32.2 N/m )

(Air-dried)
E13         0.345       6.98
E14         0.444       5.83
E17         0.345       7.98
E18         0.500       3.92
E19         0.805       1.38
E20         0.487       5.42     N = 9
E21         0.439       6.14     Y = -13.17 X + 11.73
E22         0.450       5.05     COR = -0.934
E23         0.485       6.26     J_IC = 0.239 lb/in
                                      ( 41.9 N/m )

(Saturated)
E25         0.373       7.41
E26         0.536       2.97
E27         0.684       2.15
E28         0.482       4.92
E29         0.509       4.12
E30         0.594       2.79
E31         0.786       1.79
E32         0.277      10.40
E33         0.534       3.82     N = 12
E34         0.467       3.07     Y = -15.75 X + 12.44
E35         0.465       3.59     COR = -0.858
E36         0.516       4.30     J_IC = 0.285 lb/in
                                      ( 49.9 N/m )
----------------------------------------------------------
```

Note: U = area under P-LPD from 0 to the 0.95 P_m on
      the descending branch.

      1 lb-in = 0.113 N-m
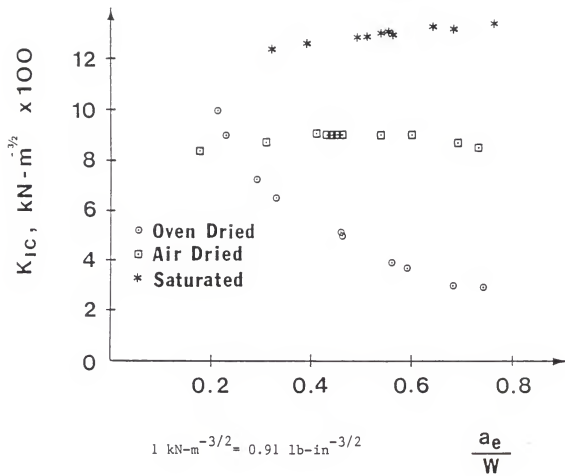
Fig. 4.1 K_{IC} vs. $\frac{a_e}{W}$ for Narrow Beams, G/R/S Method

$1 \text{ kN-m}^{-3/2} = 0.91 \text{ lb-in}^{-3/2}$
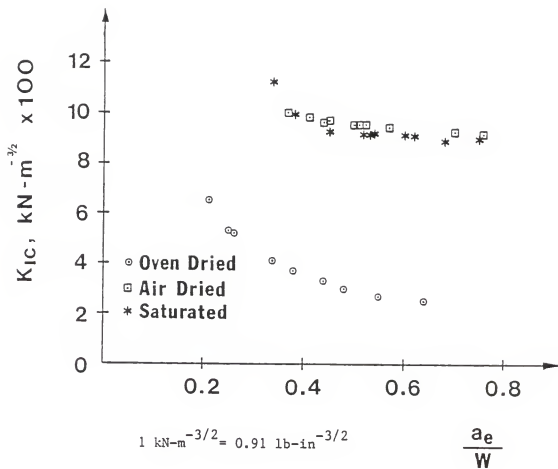
Fig. 4.2 K_{IC} vs. $\dfrac{a_e}{W}$ for Wide Beams, G/R/S Method

$1 \text{ kN-m}^{-3/2} = 0.91 \text{ lb-in}^{-3/2}$
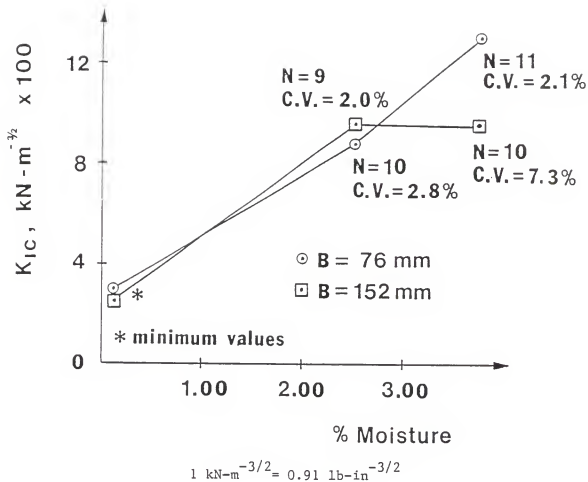
Fig. 4.3 K_{IC} vs. Moisture, G/R/S Method

$1\ kN\text{-}m^{-3/2} = 0.91\ lb\text{-}in^{-3/2}$
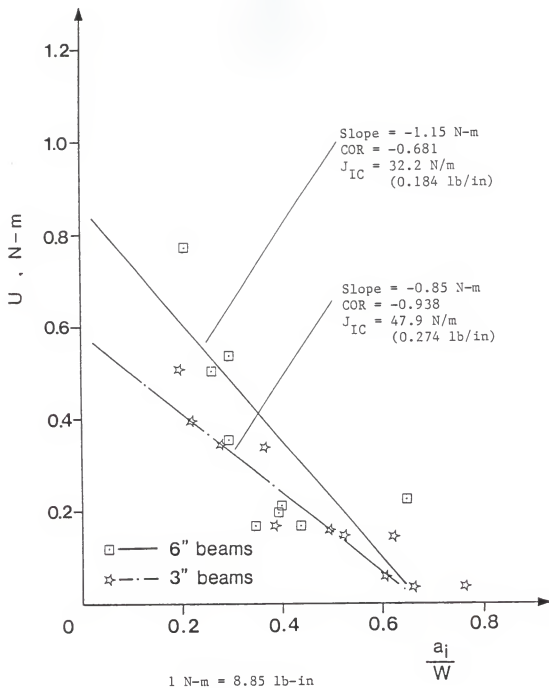
Fig. 4.4 U vs. $\frac{a_i}{W}$ for Oven-Dried Beams,
J-Integral Method
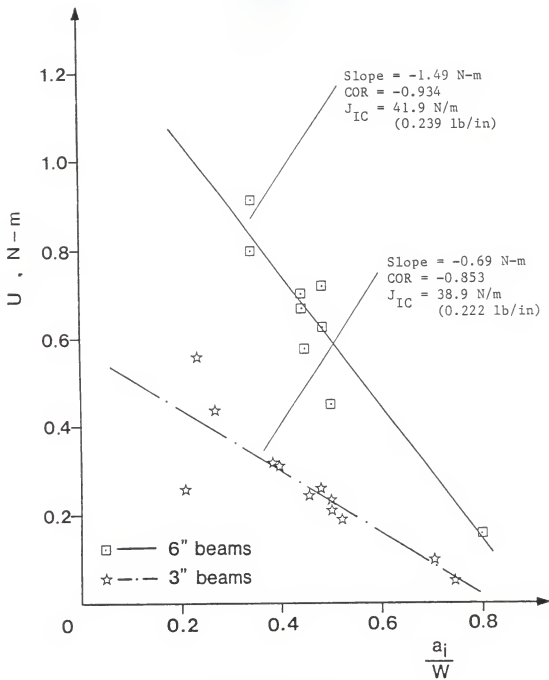
Fig. 4.5 U vs. $\frac{a_i}{W}$ for Air-Dried Beams,
J-Integral Method

1 N-m = 8.85 lb-in
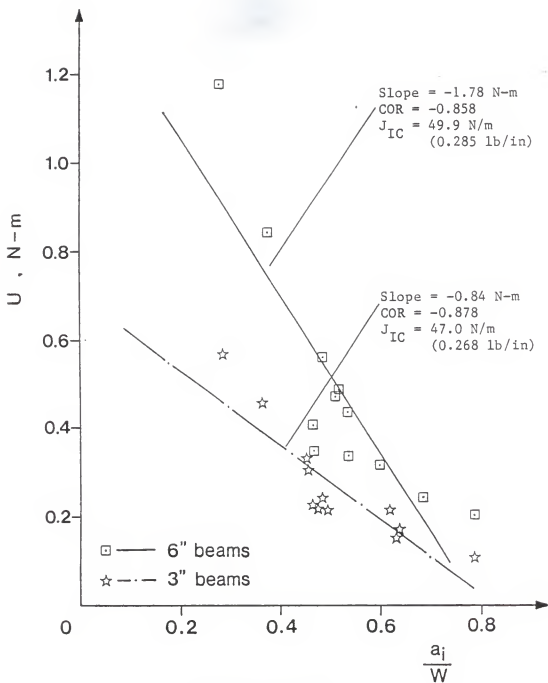
Fig. 4.6 U vs. $\frac{a_i}{W}$ for Saturated Beams,
J-Integral Method

1 N-m = 8.85 lb-in
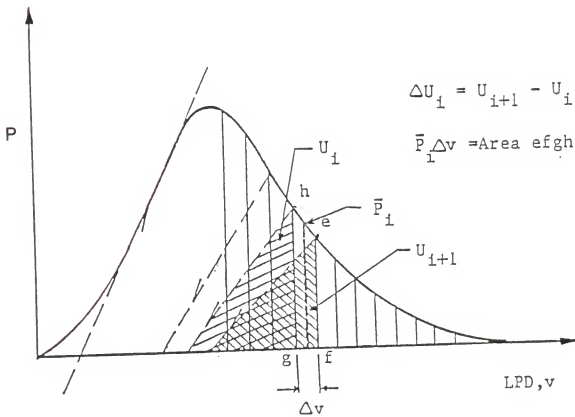
Fig. 4.7 P vs. LPD for The Energy Release Method (2)
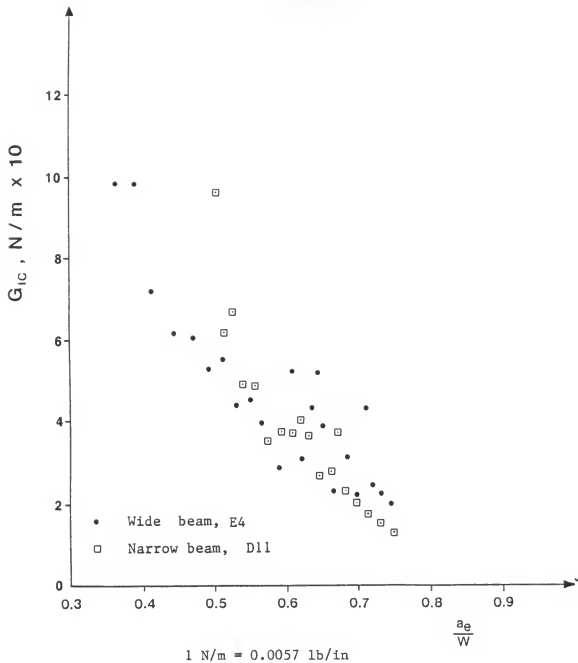
Fig. 4.8 G_{IC} vs. $\frac{a_e}{W}$ for Oven-Dried Beams

1 N/m = 0.0057 lb/in

In the figure:

Y-axis: G_{IC} , N / m × 10

X-axis: $\frac{a_e}{W}$

Legend:
- Wide beam, E4
- Narrow beam, D11
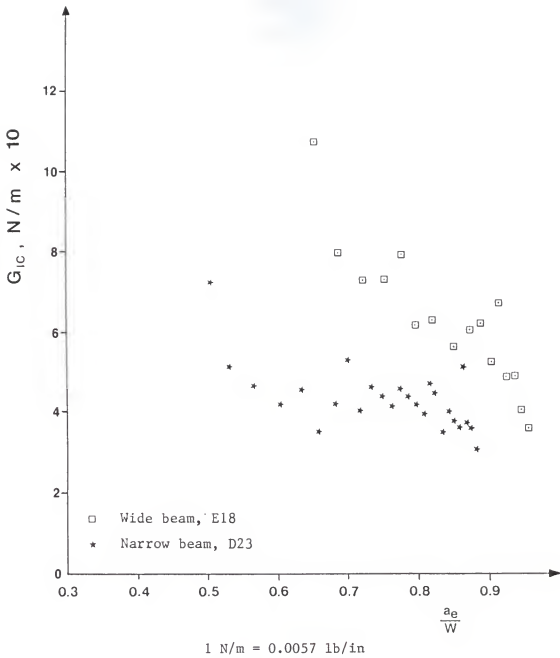
Fig. 4.9 G_{IC} vs. $\frac{a_e}{W}$ for Air-Dried Beams

$1 \text{ N/m} = 0.0057 \text{ lb/in}$

G_{IC}, N / m $\times$ 10

★ Wide beam, E34

▣ Narrow beam, D36

$\frac{a_e}{W}$

1 N/m = 0.0057 lb/in
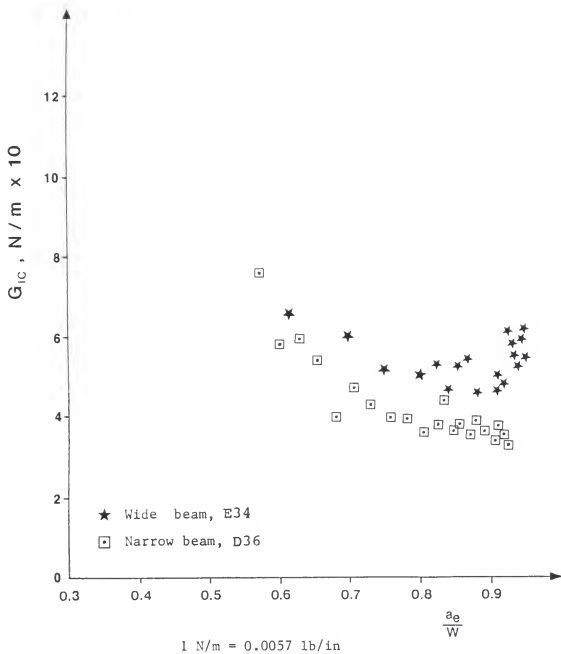
Fig.4.10 G_{IC} vs.a_e/W for Saturated Beams

CHAPTER 5

Conclusions

From the experimental results of this study, in which the influences of curing conditions and size (width) on fracture toughness values as well as energy release rates for concrete beams in three point bending were determined, the following may be concluded:

1. Oven-dried beams exhibit a size effect, but more importantly the fracture toughness K_{IC} decreases with the crack growth. The minimum value of K_{IC} is much lower than the average values for air-dried or saturated beams.

2. For the saturated beams a modest size (width) effect exists. The importance of this is open to question since most concrete structures do not exist in a saturated environment.

3. For the narrow beams a difference in results is obtained between those air-dried and those saturated. The K_{IC} values are higher for saturated beams; however, for wide beams there is no statistically-meaningful difference in results between air-dried and saturated. It seems reasonable that if a curing effect exists it would be more pronounced for the narrow beams since the region of the "side lips" occupies a greater proportion of the total area than is the case for the wide beams.

4. In general, the results obtained from the three methods used to determine K_{IC} are in agreement.

5. The values of energy release rates determined by the

J-Integral method are larger than those by fracture toughness method. This may be because of the existence of the process (plastic) zone, which consumes part of the energy, so that the explanation of the fracture on concrete using only LEFM is not sufficient.

6. From the plots of G_{IC} using the energy release method, very comparable results with those from the Go/Refai/Swartz method can be observed. For the oven-dried beams, G_{IC} varies as the crack grows, just like the trend of K_{IC} versus the crack growth shown previously. For the air-dried beams the size effect is clear. It displays a moderately invariant value for the narrow beam; while for the wide beam the G_{IC} values decrease with the increase of the crack length. For saturated beams, by selecting an appropriate range, the G_{IC} could be treated as an invariant value for both narrow and wide beams; however, size effect still exists.

References

1. Swartz, S. E. and Go, C. G., "Validity of Compliance
    Calibration to Cracked Concrete Beams in Bending,"
    Experimental Mechanics, Vol. 24, No. 2, June 1984, pp.
    129-134.

2. Refai, T. M. E. and Swartz, S. E., "Fracture Behavior
    of Concrete Beams in Three-Point Bending Considering
    The Influence of Size Effects," Report 190, Engineering
    Experiment Station, Kansas State University, Manhattan,
    KS, July 1987.

3. Swartz, S. E. and Refai, T. M. E.,"Influence of Size
    Effects on Opening Mode Fracture Parameters for
    Precracked Concrete Beams in Bending," Proceedings,
    SEM-RILEM International Conference on Fracture of
    Concrete and Rock, S. P. Shah and S. E. Swartz, ed.,
    Houston, June 17-19,1987, pp. 403-417.

4. Go, C. G. and Swartz, S. E., "Energy Methods for
    Fracture Toughness Determination in Concrete,"
    Experimental Mechanics, Vol. 26, No. 3, Sept. 1986.

5. Swartz, S. E. and Refai, T. M. E., "Cracked Surface
    Revealed by Dye and Its Utility in Determining Fracture
    Parameters," Proceedings, International Workshop on
    Fracture Toughness and Fracture Energy-Test Methods for
    Concrete and Rock, Sendai, Japan, Oct. 12-14, 1988.

6. Jenq, Y. S. and Shah, S. P., "Two-Parameter Fracture
    Model for Concrete," Journal of Engineering Mechanics,
    ASCE, Vol. 111, No. 10, Oct. 1985, pp. 1227-1241.

7. Karihaloo, B. L. and Nallathambi, P., "Notched Beam
    Test: Mode I Fracture Toughness," draft report to RILEM
    Committee 89-FMT, Fracture Mechanics of Concrete: Test
    Method, Oct. 1987.

8. Kaplan, M. F., "Crack Propagation and The Fracture of
    Concrete," Journal of the American Concrete Institute,
    Vol. 58, No. 5, November, 1961. pp.591-610.

9. Go, C. G., Swartz, S. E. and Hu, K. K., "Stress
    Intensity Factors for Single Edge Notch Beam,"
    Technical Note, Journal of Engineering Mechanics, ASCE,
    Vol. 110, No. 4, April 1984, pp. 629-632.

10. Rice, J. R., "A Path Independent Integral and The Approximate Analysis of Strain Concentration by Notches and Cracks," _Journal of Applied Mechanics_, June, 1968.

11. Hordijk, D. A. and Reinhardt, H. W., "Fracture of Concrete in Uniaxial Experiments as Influenced by Curing Conditions," International Conference on Fracture and Damage of Concrete and Rock, Vienna, July 4-6, 1988.

12. Bazant, Z. P. and Prat, Pere C., "Effect of Temperature and Humidity on Fracture Energy of Concrete," _ACI Materials Journal_, Vol. 85, No. 4. July-Aug. 1988.

13. Bazant, Z.P., "Size Effect in Blunt Fracture: Concrete, Rock, Metal," _Journal_ of Engineering Mechanics ASCE, Vol. 110, 1984, pp. 518-535.

14. Swartz, Stuart E., Hu, K. K. and Jones, Gary L. "Compliance Monitoring of Crack Growth in Concrete," _Journal_ of the Engineering Mechanics Division, ASCE, Vol. 104, No. EM4, August 1978, pp. 789-800.

15. Huang, C. L. D., Jiang, H. H. and Best, C. H., "Heat and Moisture Transfer in Concrete Slabs," _International Journal of Heat Mass Transfer_, Vol. 22, 1979, pp. 257-266.

16. Winter, G. and Nilson, A. H., _Design of Concrete Structures_, 10th ed., Chapter 2, pp. 40-41, McGraw-Hill, New York, 1986.

17. Gross, B. and Srawley, J. E., "Stress-Intensity Factors for Three-Point Bend Specimen by Boundary Collocation," NASA TN D-3092, 1965.

18. Broek, D., _Elementary Engineering Fracture Mechanics_, Chapter 5, pp. 123-128, Martinus Nijhoff Publishers, The Hague, 1986.

APPENDIX   II

LOAD VERSUS CMOD AND LPD DIAGRAMS FOR
TYPICAL THREE-POINT BENDING SPECIMENS
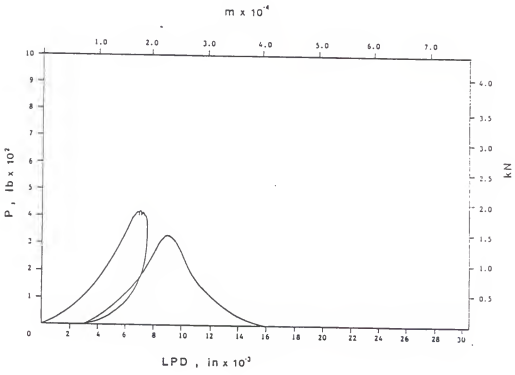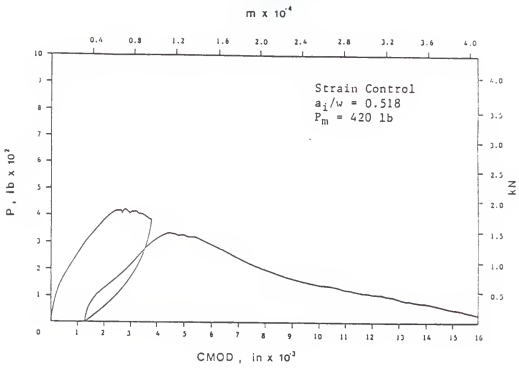
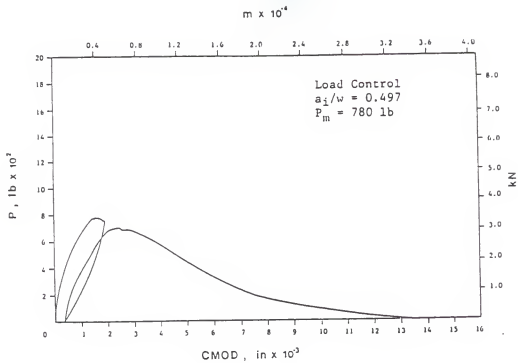Fig. 1 Load vs. CMOD and LPD for D11,
Oven-Dried, Narrow Beam
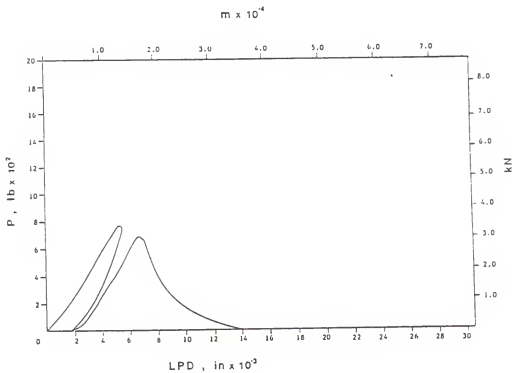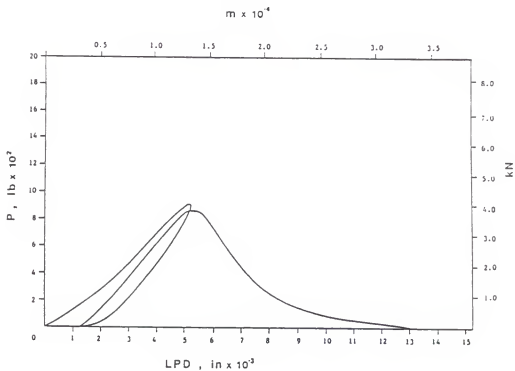
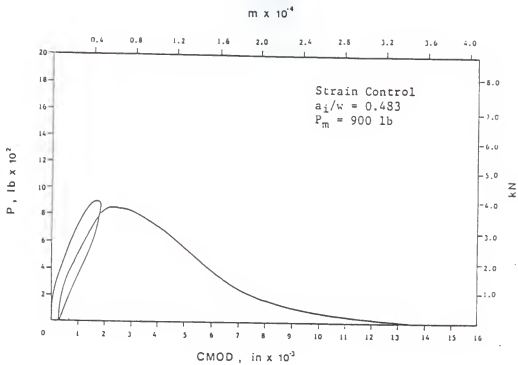Fig. 2 Load vs. CMOD and LPD for D23,
Air-Dried, Narrow Beam

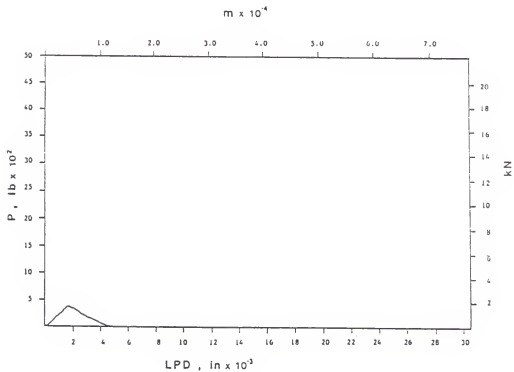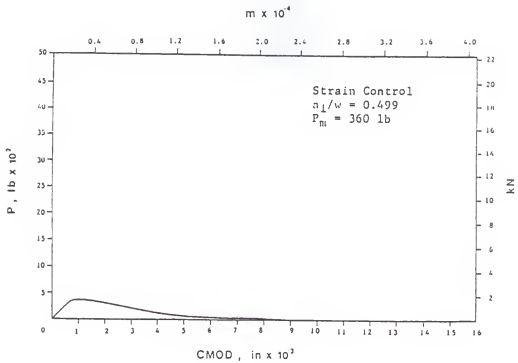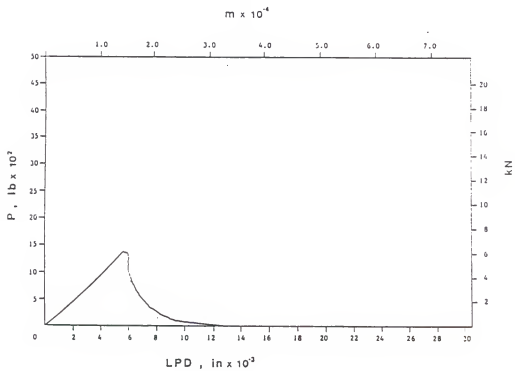Fig. 3 Load vs. CMOD and LPD for D36,
Saturated, Narrow Beam

m x 10⁻⁴

Strain Control
$a_1/w = 0.499$
$P_m = 360$ lb

P , lb x 10²

kN

CMOD , in x 10³

m x 10⁻⁴

P , lb x 10²

kN

LPD , in x 10³

Fig. 4 Load vs. CMOD and LPD for E6,
Oven-Dried, Wide Beam
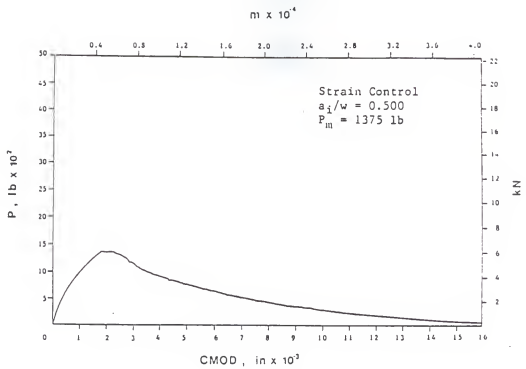
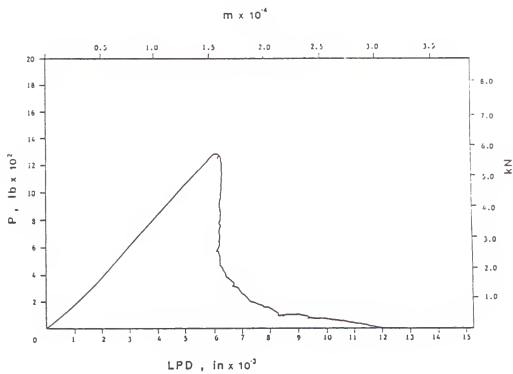Fig. 5 Load vs. CMOD and LPD for E18,
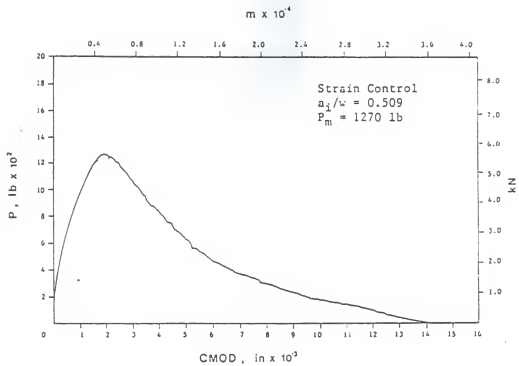Air-Dried, Wide Beam

Fig. 6   Load vs. CMOD and LPD for E29,
Saturated, Wide Beam

INFLUENCE OF CURING CONDITIONS AND WIDTH

ON THE FRACTURE OF CONCRETE BEAMS

by

Yu-Cheng Kan

B.S.. Chung-Hsing University, Taiwan, 1985

AN ABSTRACT OF A MASTER'S THESIS

submitted in partial fulfillment of
the requirements for the degree of

MASTER OF SCIENCE

Department of Civil Engineering

Kansas State University

Manhattan, Kansas

1989

ABSTRACT

Although a large amount of research has been reported in the literature dealing with curing conditions on the subsequent strength of concrete, few studies have been conducted relating these effects to the fracture properties of concrete, such as fracture toughness and the critical energy release rate. Most of the fracture mechanics tests were done using either saturated or air-dried specimens.

Thirty six beams in two series of 3x8x34 in. and 6x8x34 in. with S/W of 4 were utilized in this experimental program based on the three-point bend tests. The curing conditions were: 1 day in the mold, 30 days in a 100% humidity curing room for all specimens and then for each beam series

    a. 12 beams, 60 days in an oven at 177°F,

    b. 12 beams, 60 days in the laboratory environment,

    c. 12 beams, 60 additional in the curing room.

All beams were precracked and a dye technique was applied. Through the use of three proposed methods, based on LEFM, the fracture toughness and energy release rate could be calculated. As a result, the fracture toughness evaluated by the three methods was found to be independent of the crack length and approximately independent of beam width and curing condition for the air-dried and saturated beams but not for the oven-dried beams. In addition, two other methods for determining the energy release rates were also used to compare with the above results.